Reevaluating GPR30: A Paradigm Shift from Estrogen Receptor to Unique Hydrophilic Ligand Activation

Heng Liu[1,8], Shimeng Guo[1,8], Antao Dai[2,8], Peiyu Xu[1,8], Xin Li[1,3], Sijie Huang[1], Xinheng He[1,3], Kai Wu[1,4], Xinyue Zhang[1], Dehua Yang[2,3*], Xin Xie[1,3,5,6*], H. Eric Xu[1,3,7*]

[1]The State Key Laboratory of Drug Research, Shanghai Institute of Materia Medica, Chinese Academy of Sciences, Shanghai 201203, China

[2]The State Key Laboratory of Chemical Biology, Shanghai Institute of Materia Medica, Chinese Academy of Sciences, Shanghai 201203, China

[3]University of Chinese Academy of Sciences, Beijing 100049, China

[4]The Shanghai Advanced Electron Microscope Center, Shanghai Institute of Materia Medica, Chinese Academy of Sciences, Shanghai 201203, China

[5]School of Pharmaceutical Science and Technology, Hangzhou Institute for Advanced Study, University of Chinese Academy of Sciences, Hangzhou, China

[6]Shandong Laboratory of Yantai Drug Discovery, Bohai Rim Advanced Research Institute for Drug Discovery, Yantai, China

[7]School of Life Science and Technology, ShanghaiTech University, Shanghai 201210, China

[8]These authors contributed equally

*Correspondence: dhyang@simm.ac.cn (D.Y.), xxie@simm.ac.cn (X.X.), eric.xu@simm.ac.cn (H.E.X.)

Abstract

The orphan receptor GPR30, previously classified as a G protein-coupled estrogen receptor (GPER), has been a subject of debate regarding its ligand specificity. Through an integrative approach combining structure elucidation, biochemical binding, and cell signaling assays, we demonstrate that estrogen does not directly bind to or activate GPR30. Cryo-EM structures of GPR30 reveal an unexpected hydrophilic ligand-binding pocket, with striking differences from classical hydrophobic steroid-binding sites, inconsistent with estrogen binding. We further confirmed hydrophilic agonists like Lys05 as true activators of GPR30, providing structural insights into their binding mechanism and receptor activation. Our findings necessitate a paradigm shift in defining GPR30's role in estrogen signaling, indicating that its activation occurs through mechanisms independent of estrogen binding. This study opens new avenues for developing targeted GPR30 ligands and reinterpreting its role in estrogen-mediated processes.

Introduction

Estrogen is a pivotal hormone in human physiology, orchestrating a wide range of biological processes ranging from reproductive functions to cardiovascular health and bone integrity[1-3]. Its effects are traditionally understood to be mediated through nuclear estrogen receptors, ERα[4] and ERβ[5,6], which function as transcription factors regulating gene expression[1-4]. However, the rapid, non-genomic actions of estrogen imply the existence of membrane-associated estrogen receptors enabling swift cellular responses[7-9]. G protein-coupled estrogen receptor (GPER)[10], also known as GPR30[11-14], was identified as one such candidate over 18 years ago[15,16]. Initial studies reported that GPR30 binds estrogen[15,16] and mediates rapid estrogen signaling through various pathways[15-18], including downstream pathways mediated by the G protein subtype, Gq[19], which induces the generation of the second message, inositol phosphate IP1, leading to activation of PKC and calcium signaling. This sparked great interest and debate over the role of GPR30 in estrogen physiology[20,21].

The discovery of GPR30 as a novel estrogen receptor (GPER) has provided a mechanism of the rapid action of estrogen via GPR30 and facilitated the development of GPR30 modulators[20]. While the endogenous ligand 17β-estradiol (E2) activates GPR30[15,16], selective estrogen receptor antagonists like tamoxifen[22,23] and raloxifene[24], ER-degrading agent fulvestrant[16], have also been reported to display GPR30 agonism. Additionally, several synthetic ligands, including G-1[25], were reported to be selective GPR30 agonists.

However, subsequent studies have produced inconsistent results about whether GPR30 truly serves as an estrogen receptor with independent signaling capacity from nuclear estrogen receptors[19,26-37]. A recent unbiased screen found no activation of GPR30 by estrogen, 4-hydroxytamoxifen, or the selective GPR30 agonist G-1 in cells overexpressing GPR30, confounding GPR30 as a bona fide estrogen receptor. Instead, it identified chlorhexidine, Lys05, and 9-aminoacridine as potent GPR30 activators[19].

Furthermore, knocking down GPR30 in MCF-7 cells expressing estrogen receptors (ERs) and GPR30 showed no impact on E2-induced the generation of cyclic AMP (cAMP), the second message downstream of Gs activation, but E2-induced cAMP production is affected by double knockout of ERα and ERβ[26]. The presence of membrane ERs (mERs)[38], albeit at a limited level of about 3-10% of classical nuclear ERs, which are reported to co-operate with GPR30[29], further complicated the rapid non-genomic signaling events mediated by E2[33]. There is also evidence that G-1 may signal through estrogen receptor variants ERα-36 and ERα-46 instead of GPR30[31,39-41]. In addition, rapid signaling by estrogen at the plasma membrane is absence in ER negative but GPR30 positive cells [26]. Clearly, definitive evidence for direct estrogen binding and signaling by GPR30 is still lacking and controversial[28,34].

In this paper, we combined biochemical, structural, and functional approaches to directly test whether GPR30 interacts with and signals in response to estrogen and estrogen-related compounds. We determined cryo-EM structures of GPR30 bound to Gq in the presence of high concentrations of estrogen and its related ligands, G-1 and fulvestrant, however, none of these compounds was found in these GPR30 structures. Functional and radioligand binding assays were consistent with the structural data that show no direct GPR30-estrogen interaction. In contrast, the hydrophilic ligand, Lys05, was found to bind to the orthosteric pocket of GPR30, revealing a unique mechanism of GPR30 activation independent of estrogen binding. By definitively demonstrating GPR30 is not a membrane estrogen receptor, our integrative study fundamentally shifts thinking and necessitates reinterpreting GPR30's contributions to estrogen biology.

Cryo-EM structures contradict GPR30 as a direct estrogen receptor

GPR30 was hypothetically conceived as a G protein-coupled estrogen receptor that directly binds estrogen, offering mechanisms explaining non-genomic effects and tissue-selectivity of estrogen signaling. This provocative idea has profoundly impacted on our comprehension of rapid estrogen biology. Thus, we initially aimed to use

structural biology, specifically cryo-EM, a technique successfully applied in numerous GPCR-ligand studies[42-47], to visualize estrogen binding directly to GPR30.

For our cryo-EM studies, we engineered the human GPR30 by appending a haemagglutinin (HA) signal peptide, FLAG, and His tags for expression and purification, and introduced a BRIL fusion tag at the N-terminus to enhance complex stability (Fig. S1). We utilized an engineered Gαq (see Methods), shown effective in mimicking Gαq-coupled GPCR activation in various receptors, like growth hormone secretagogue receptor (GHSR)[48]. Co-expression of GPR30 with this engineered Gαq, along with rat Gβ1, bovine Gγ2, and scFv16 in Hi5 insect cells, allowed us to form stable GPR30-Gq complexes in the presence of E2, G1, or fulvestrant (Fig. S1).

We determined structures of GPR30-Gq complexes with saturated concentrations of E2, the selective agonist G-1, and the ER-degrader fulvestrant at 3.1-3.2 Å resolution (Fig. S1, Fig. S2, Table S1). In all structures, GPR30 adopts an active-like state typical of GPCR-G protein coupling. Surprisingly, despite relatively high resolutions of the structures, no ligand density was observed in the GPR30 binding pocket (Fig. 1A-B). We additionally solved an apo-GPR30-Gq structure at 2.9 Å resolution (Fig. 1C, Fig. S2, Table S1). Structural alignments reveal a striking similarity between GPR30 conformations in the presence or absence of added ligands, with root mean square deviation (RMSD) values of just 0.373 Å, 0.378 Å and 0.368 Å when comparing structures solved with E2, G-1, or fulvestrant, to the apo-GPR30-Gq complex, underscoring the highly analogous states regardless the presence of these compounds (Fig. S3A). A comparison of the EM structures with the AlphaFold[49] structure showed overall concordance yet revealed notable local discrepancies in positioning of transmembrane helices, particularly having 3-4 Å differences in the extracellular regions of TM1, TM2, and TM3 (Fig. 1D), indicating that even for recurrence fold such as GPCRs, AlphaFold prediction can still deviated greatly from experimental structures[50].

Notably, examining GPR30's pocket architecture reveals a striking hydrophilic nature enriched with negatively charged residues (Fig. 1E-F). This clashes with accommodating hydrophobic estrogen ligands (Fig. S3B), which is in contrast with related steroid hormone receptors with hydrophobic pockets as indicated in ERα, ERβ, and several steroid binding GPCRs (Fig. S3C). In addition, the GPR30 pocket is much larger than the corresponding pocket for steroid-related ligands (Fig. S3D). This spacious GPR30 cavity also seems unsuitable for smaller estrogen binding. Together, these inconsistencies argue that estrogen is unlikely the cognate ligand as originally hypothesized based on the cryo-EM structural evidence we established. In the next sections, we provide further biochemical and functional evidence that estrogen is not a direct ligand of GPR30.

Functional assays challenge GPR30 as a direct estrogen receptor

Our structural findings challenge the proposed concept of GPR30 as a membrane estrogen receptor. We further investigated this through binding experiments and signaling analyses.

First, we performed the competitive radioligand binding assays using [^{3}H]17β-estradiol ([^{3}H]-E2) (Fig. 2A) with CV1 cells expressing GPR30 or ERα. As anticipated and in alignment with existing literature[51], ERα-transfected cells exhibited high-level binding to [^{3}H]-E2 that can be specifically competed by addition of unlabeled E2 (Fig. 2B). Conversely, [^{3}H]-E2 showed low basal-level binding to GPR30-transfected cells (similar to empty cells) in the presence or absence of increasing concentrations of unlabeled E2 (Fig. 2B). E2-related ligands such as tamoxifen and raloxifene (Fig. 2A) can also effectively compete with [^{3}H]-E2 in binding to ERα but did not affect the nonspecific binding of [^{3}H]-E2 on GPR30 (Fig. 2C-D). We recapitulated these results with [^{3}H]-E2 binding to the membrane from Hi5 cells overexpressing GPR30 and ERα,

and the consistent results further reinforce the lack of direct GPR30-estrogen interaction (Fig. S4A).

In cell-based functional assays, E2 elicited no changes of cAMP or IP1 in GPR30-expressing cells at concentrations up to 100 μM, indicating no stimulation of Gs or Gq pathways (Fig. 2E, F). E2 did not reduce the cAMP levels promoted by forskolin either, indicating no activation of Gi pathway (Fig. 2G) In contrast, the recently identified GPR30 agonist Lys05 (Fig. 2A) induced dose-dependent accumulation of IP1 without affecting cAMP levels (Fig. 2E-G), consistent with the knowledge that GPR30 dominantly couples to Gq[19]. Lys05 also induced calcium flux in GPR30 expressing cells with an EC_{50} value of ~462 nM, a response not observed with E2-related compounds or in parental HEK293 cells (Fig. S4B-C), consistent with activation of the Gq-IP1-calcium pathway. Together, our integrated binding and functional data clear indicate that GPR30 is not an estrogen receptor.

Structure of GPR30 bound to Lys05

Our functional assays have established that Lys05, a molecule characterized by multiple positively charged nitrogen atoms (Fig. 2A), effectively activates GPR30, initiating downstream signaling through the Gq pathway (Fig. 2E, Fig. S4B-C). Intrigued by this interaction, particularly given GPR30's negatively charged ligand-binding pocket (Fig. 1E), we embarked on a detailed structural investigation.

We successfully determined the high-resolution structure of the Lys05-GPR30-Gq complex at an overall resolution of 2.6 Å (Fig. 3A, Fig. S5). This resolution enabled us to resolve the entire structure, including the transmembrane helices, intracellular loops, and the Gq heterotrimer. Most notably, we observed a distinct EM density for Lys05 within the GPR30 binding site (Fig. 3A), in stark contrast to our previous GPR30 structures solved in the presence of E2 and related compounds (Fig. 1A-B).

In the Lys05-bound state, the ligand is nestled within a pocket formed by TM2, TM3, TM6, and TM7. This pocket is enriched with negatively charged residues, aligning perfectly with Lys05's structure (Fig. 3B), which features two hydrophobic ends linked by a positively charged segment (Fig. 2A). This spatial arrangement highlights the specificity of Lys05 binding to GPR30.

A comparative analysis between the apo-GPR30 and Lys05-activated GPR30 structures revealed a similar activated conformation (Fig. S5G). The RMSD values for the entire complex were 1.223 Å and 0.326 Å for the receptor alone, indicating a high degree of structural similarity. Upon closer inspection, we noted that TM3 and TM5 in the Lys05-bound structure underwent inward shifts compared to their positions in the apo structure. Specifically, TM3 shifted by approximately 0.9 Å (Cα of T131^{3x26}) and TM5 by around 2.5 Å (Cα of E213^{5x37}), suggesting ligand-induced conformational changes (Fig. S5G).

Structural analysis reveals a unique distribution of the transmembrane region of GPR30. Notably, TM1 and TM4 arrangements in GPR30's 7TM bundle deviate from amine/steroid receptors, such as serotonin receptor, $5HT_{1A}$[52] and G protein-coupled bile acid receptor, GPBAR[53] (Fig. S6A), but match better with peptide-activated GPCRs like GHSR[48] and neuromedin U receptor 2 (NMUR2)[54] (Fig. S6B). This architecture likely accommodates the Lys05's linear amine linker. Overall, the Lys05-bound GPR30 structure provides molecular insights into ligand interactions enabling pharmacological targeting of GPR30's distinctive ligand binding pocket.

Molecular Recognition of Lys05 by GPR30

The relatively high-resolution structure of Lys05 coupled with an activated GPR30 conformation has elucidated the ligand recognition mechanisms in detail (Fig. 4A). For analysis, we designated the nitrogen atoms in Lys05's symmetrical structure as N1 through N5, from the bottom to the top of the ligand structure. Lys05 inserts into the

orthosteric pocket lined by TM2, TM3, TM6, and TM7, engaging with the receptor through a tri-layered interface (Fig. 4A).

At the bottom of the binding pocket, the insertion of Lys05 rearranges L137^{3x32} and M141^{3x36}. Specifically, L137^{3x32} flips towards TM2, while M141^{3x36} rotates approximately 50° away (Fig. S7A). This rearrangement gives rise to a hydrophobic sub-binding pocket consisting of L108^{2x53}, L137^{3x32}, M141^{3x36}, W272^{6x48}, A313^{7x42}, and F314^{7x43} (Fig. 4A-B). To underscore the importance of these hydrophobic contacts, we introduced alanine mutations at these sites and assessed their impact on Lys05 activity. Strikingly, alanine substitution at any of these residues, including L108^{2x53}A, L137^{3x32}, M141^{3x36}, W272^{6x48}, and F314^{7x43}, nearly abolished activation by Lys05 (Fig. 4C, Fig. S7), without affecting GPR30 surface expression (Table. S2). These data suggest the crucial role of the hydrophobic sub-pocket in stabilizing Lys05.

At the center of the pocket is a hydrophilic layer, where the positively charged N2 and N3 amines of Lys05 form polar contacts with E115^{2x60}, Q138^{3x33}, E275^{6x51} and N310^{7x39} (Fig. 4A, 4D). Specifically, E115^{2x60} forms polar interactions with the N2 amine of Lys05, while N310^{7x39} and E275^{6x51} form polar interactions with the N3 amine of Lys05 (Fig. 4D). Critically, the N2 and N3 amines provide essential positive charges for the accommodation of the surrounding negatively charged pocket (Fig. 4A). As expected, E115^{2x60}A and Q138^{3x33}A mutations eliminated activation, while E275^{6x51}A reduced potency by approximately ten-fold (Fig. 4C, Fig. S7, Table. S2).

The top of the pocket is a hydrophobic layer that involves weaker interactions between the top tryptamine moiety of Lys05 and residues from TM6 and ECL3 of GPR30, engaging H300^{ECL3}, H282^{6x58}, and P303^{7x32} (Fig. 4E). Mutations in these amino acids mildly impacted activation (Fig. 4C, Fig. S7, Table. S2), suggesting their auxiliary role in Lys05 recognition.

Activation mechanisms of GPR30

In the cryo-EM map of the apo-GPR30 Gq structure, several structured waters clearly form hydrogen-bonding interactions within the orthosteric pocket. Specifically, two well organized water molecules, denoted as W1 and W2, are solved to a local resolution of approximately 3.0 Å (Fig. S2K), are hypothesized to potentially play a role in GPR30's self-activation. These water molecules, positioned in proximity to the negatively charged pocket core, actively engage in hydrogen bonds with key residues (Fig. 5A-B). W1's positioning and interactions, particularly with E115^{2x60}, E275^{6x51}, and N310^{7x39}, coincide with the tryptamine group of Lys05 (Fig. 5C). Meanwhile, W2 establishes hydrogen bonds with E275^{6x51} and E218^{5x42} (Fig. 5A-C). These water-mediated contacts appear to mimic ligand interactions, promoting GPR30's adoption of an active-like state, offering insights into potential basal activation mechanisms of GPR30.

In the absence of an inactive GPR30 structure, we conducted a comparison with the inactive κ-opioid receptor (KOR)[55], which displays one of the highest sequence similarities among all GPCRs, to GPR30. This comparison between active and inactive GPCR states illuminated the activation mechanism of GPR30. Notably, the active GPR30 structures demonstrate typical rearrangements characteristic of activated GPCRs, such as the agonist-induced outward movement of TM6 at the cytoplasmic side, similar to changes observed in KOR[56] (Fig. 5D).

In the Lys05-GPR30-Gq complex, the binding of Lys05 exerts pressure on the W272$^{6\times48}$ toggle switch, triggering a cascade of conformational shifts (Fig. 5E). This interaction induces alterations in the F268$^{6\times44}$-V145$^{3\times40}$ of PIF motif and R155$^{3\times50}$ of the DRY motif, ultimately disrupting the ionic lock between TM3 and TM6. As a result, TM6 moves outward by approximately 6.2 Å at the R254$^{6\times30}$ Cα position. Concurrently, TM7's cytoplasmic portion shifts inward by about 2.7 Å (Fig. 5D). This inward movement allows Y324$^{7\times53}$ of NPxxY motif residues, and Y234$^{5\times58}$, to form hydrogen

bonds with R155$^{3\times50}$ of DRY (Fig. 5F-H). These coordinated structural changes facilitate the opening of the cytoplasmic pocket, priming GPR30 for effective coupling of downstream G protein.

Gq coupling of GPR30

Structural comparisons of the GPR30-Gq complex with other Gq/11-coupled class A GPCRs[46,54] reveal a broadly parallel coupling mechanism. However, our analysis identified a distinctive feature in GPR30's coupling with Gαq, particularly in the positioning of the αH5 helix of the Gαq protein (Fig. 6A). In the GPR30-Gq complex, the N-terminus of αH5 is positioned closer to the junction of TM5 and TM6 in GPR30, diverging by approximately 15° compared to other Gq-coupled receptors such as GSHR[48], NMUR2[54] and CCKAR[57] (Fig. 6A). This unique orientation may reflect the specific activation characteristics of GPR30, which induces a comparatively smaller displacement of TM6 (Fig. 6A).

The interaction between GPR30 and Gαq involves two critical regions of the receptor: the engagement of the Gαq α5 helix by TM3, TM5, TM7, and H8 of GPR30, and interactions mediated by GPR30's intracellular loops (ICLs) (Fig. 6B). The major interface is formed by the distal αH5 region of Gαq and the intracellular receptor cavity. Key hydrophobic and polar interactions at this interface include:1) a hydrophobic stack between V394$^{G.H5.26}$, L393$^{G.H5.25}$, L388$^{G.H5.20}$, L384$^{G.H5.16}$, I383$^{G.H5.15}$ on Gαq α5 helix, and GPR30 residues L159^{3x54}, L241^{5x65}, A356^{6x33}, M260^{6x36}, I261^{6x37}; 2) polar interactions such as the Q385$^{G.H5.17}$ - R254^{6x30} hydrogen bond and N392$^{G.H5.24}$ interacting with T330^{8x49} in helix 8 and backbone of S325^{7x54} (Fig. 6B-C).

Significant ICL2-Gαq interactions are also observed, including the insertion of M163^{34x51} into a hydrophobic cavity on Gαq. This interaction is reminiscent of those seen in other Gq-GPCRs[48,54,57] (Fig. 6B and 6D). Additionally, R169^{34x57} forms a polar interaction with E390$^{G.H5.22}$, with its backbone carboxyl group interacting with R38 on

αN of Gαq. R164^{34x52} establishes a hydrogen bond with the D215 backbone of Gαq.

A unique aspect of the GPR30-Gq structure is the increased interaction between TM6-ICL3 of GPR30 and Gαq, facilitated by a smaller outward movement of TM6 in GPR30 (Fig. 6A). Notably, R254^{6x30} on GPR30 forms a stabilizing interaction with Q385$^{G.H5.17}$ and D381$^{G.H5.13}$ on Gαq αH5. Furthermore, R248^{ICL3} forms a salt bridge with D378$^{G.H5.10}$ on αH5 (Fig. 6E). These additional contacts, unique to the GPR30-Gq complex, highlight the distinct conformational adaptations of GPR30 in its coupling with Gαq.

Discussion

The study of estrogen signaling is pivotal for understanding a wide range of physiological processes, from reproductive health to neurological functions[1,3]. GPR30, previously conceptualized as a membrane estrogen receptor (GPER)[10], has been central to discussions about rapid, non-genomic estrogen responses[20,21]. However, our comprehensive structural, biochemical, and functional analyses necessitate a fundamental shift in understanding GPR30's role. We have clearly demonstrated that GPR30 does not directly bind or get activated by estrogen, thereby challenging its classification as a direct membrane estrogen receptor.

The cryo-EM structures of GPR30 revealed no density for E2, G-1, or the ER-degrader fulvestrant. Instead, the orthosteric pocket of GPR30 exhibits a hydrophilic nature, unsuitable for binding of hydrophobic steroid hormones like estrogen. This finding aligns with our radioligand binding assays, which also indicates no specific estrogen binding to GPR30. Consequently, we must reinterpret GPR30's role in estrogen signaling, considering indirect mechanisms or completely estrogen-independent functions of this receptor.

The definitive exclusion of GPR30 as a membrane estrogen receptor redirects our focus

to other potential mediators of rapid estrogen responses. Candidates like ERα-36[40], ERα-46[41] and membrane-associated ERs (mERs) warrant further investigation to understand their roles and interactions in membrane-initiated signaling[29,31,33]. Clarifying the crosstalk or cooperation between these receptors and GPR30 could provide deep insights into estrogen's complex signaling pathways.

The nature of GPR30's native ligand remains an open question, especially since estrogen is now excluded. The hydrophilic pocket architecture of GPR30 and the unique arrangement of its 7TM bundle suggest an affinity for ligands differing from traditional hydrophobic steroids. We have successfully characterized Lys05, a synthetic small molecule, which activates GPR30 and the downstream Gq signaling pathway. The extensive interactions between Lys05 and GPR30, as revealed by our structural analysis, advance our understanding of GPR30’s activation and signaling mechanisms.

Our findings have significant implications for the field of hormone signaling and the study of GPCRs. The discovery that GPR30 does not act as a direct estrogen receptor calls for a reconsideration of its nomenclature. Referring to GPR30 as GPER may no longer be appropriate, considering its distinct ligand-binding and activation properties. This study lays the groundwork for developing new tools to probe GPR30's function, potentially leading to a better understanding of its physiological roles and its connections to estrogen biology. Unraveling these mechanisms will offer profound insights into hormone signaling complexities and pave the way for innovative therapeutic approaches targeting GPR30.

Acknowledgements

This work was supported by grants from the National Natural Science Foundation of China (82121005 to X.X., H.E.X. and D.Y., 32130022 to H.E.X., 82330113 to X.X., 82273985 to D.Y., 82304579 to S.G.); CAS Strategic Priority Research Program (XDB37030103 to H.E.X.); Shanghai Municipal Science and Technology Major Project (2019SHZDZX02 to H.E.X.); Shanghai Municipal Science and Technology Major Project (H.E.X.); the Lingang Laboratory, Grant No.LG-GG-202204-01 (H.E.X.); the National Key R&D Program of China (2022YFC2703105 to H.E.X.). Shanghai Municipality Science and Technology Development Fund 21JC1401600 (D.Y.) and Program of Shanghai Academic/Technology Research Leader 23XD1400900 (D.Y.). The cryo-EM data were collected at the Shanghai Advanced Electron Microscope Center, Shanghai Institute of Material Medica and the electron microscopy facility of Shanghai Institute of Materia Medica (SIMM), Chinese Academy of Sciences. We thank Q. Yuan., K. Wu., W. Hu., S. Li. and S. Zhang. for providing technical support and assistance during data collection at the Shanghai Advanced Electron Microscope Center, Shanghai Institute of Material Medica. We thank all staff from the electron microscopy facility of SIMM for their support.

Author contributions

H.E.X. and P.X. initiated the project. H.L. designed and screened the expression constructs of GPR30 and prepared protein samples of apo-GPR30-Gq, Lys05-GPR30-Gq complexes for cryo-EM data collection, performed cryo-EM grids preparation, data acquisition, structure determination and model building, and prepared the draft of the manuscript and figures. S.G. performed cell-based function assay and participated in figure preparation. A.D. performed the radioligand binding assay. P.X. designed and screened the expression constructs of GPR30 and prepared protein samples of GPR30-Gq complexes in the presence of E2, G1 and fulvestrant for cryo-EM data collection, performed cryo-EM grids preparation, data acquisition and participated in structure determination. K.W. participated in sample screening and data collection. S.H. and X.Z.

participated in protein samples preparation and structure determination. Y.L. participated in cell-based function assay. X.H. participated in figures preparation. D.Y. supervised the radioligand binding assay. X.X. supervised the cell-based function assay. H.E.X., X.X., and D.Y. conceived and supervised the overall project and participated in manuscript editing. H.E.X. wrote the manuscript with inputs from all authors.

Data availability

Density maps and structure coordinates have been deposited in the Electron Microscopy Data Bank (EMDB) and the Protein Data Bank (PDB) with accession codes EMD-38527 and 8XOF for Lys05-GPR30-Gq complex; EMD-38528 and 8XOG for apo-GPR30-Gq complex; EMD- EMD-38529 and 8XOH for GPR30-Gq complex in the presence of E2; 8XOI for GPR30-Gq complex in the presence of fulvestrant; and EMD-38531 and 8XOJ for GPR30-Gq complex in the presence of G1; Source data is provided with this paper.

Competing interests

The authors declare no competing interests.

References

1. Cui, J., Shen, Y. & Li, R. (2013). Estrogen synthesis and signaling pathways during aging: from periphery to brain. Trends Mol Med 19, 197-209.
2. Fuentes, N. & Silveyra, P. (2019). Estrogen receptor signaling mechanisms. Adv Protein Chem Struct Biol 116, 135-170.
3. Chen, P., Li, B. & Ou-Yang, L. (2022). Role of estrogen receptors in health and disease. Front Endocrinol (Lausanne) 13, 839005.
4. Walter, P., Green, S., Greene, G., Krust, A., Bornert, J. M., Jeltsch, J. M., et al. (1985). Cloning of the human estrogen receptor cDNA. Proc Natl Acad Sci U S A 82, 7889-7893.
5. Mosselman, S., Polman, J. & Dijkema, R. (1996). ER beta: identification and characterization of a novel human estrogen receptor. FEBS Lett 392, 49-53.
6. Kuiper, G. G., Enmark, E., Pelto-Huikko, M., Nilsson, S. & Gustafsson, J. A. (1996). Cloning of a novel receptor expressed in rat prostate and ovary. Proc Natl Acad Sci U S A 93, 5925-5930.
7. Szego, C. M. & Davis, J. S. (1967). Adenosine 3',5'-monophosphate in rat uterus: acute elevation by estrogen. Proc Natl Acad Sci U S A 58, 1711-1718.
8. Pietras, R. J. & Szego, C. M. (1975). Endometrial cell calcium and oestrogen action. Nature 253, 357-359.
9. Pietras, R. J. & Szego, C. M. (1979). Estrogen receptors in uterine plasma membrane. Journal of Steroid Biochemistry 11, 1471-1483.
10. Alexander, S. P. H., Mathie, A. & Peters, J. A. (2008). Guide to Receptors and Channels (GRAC), 3rd edition. British Journal of Pharmacology 153, S1-S1.
11. Feng, Y. & Gregor, P. (1997). Cloning of a novel member of the G protein-coupled receptor family related to peptide receptors. Biochem Biophys Res Commun 231, 651-654.
12. Owman, C., Blay, P., Nilsson, C. & Lolait, S. J. (1996). Cloning of human cDNA encoding a novel heptahelix receptor expressed in Burkitt's lymphoma and widely distributed in brain and peripheral tissues. Biochem Biophys Res Commun 228, 285-292.
13. Takada, Y., Kato, C., Kondo, S., Korenaga, R. & Ando, J. (1997). Cloning of cDNAs encoding G protein-coupled receptor expressed in human endothelial cells exposed to fluid shear stress. Biochem Biophys Res Commun 240, 737-741.
14. Kvingedal, A. M. & Smeland, E. B. (1997). A novel putative G-protein-coupled receptor expressed in lung, heart and lymphoid tissue. FEBS Lett 407, 59-62.
15. Revankar, C. M., Cimino, D. F., Sklar, L. A., Arterburn, J. B. & Prossnitz, E. R. (2005). A transmembrane intracellular estrogen receptor mediates rapid cell signaling. Science 307, 1625-1630.
16. Thomas, P., Pang, Y., Filardo, E. J. & Dong, J. (2005). Identity of an estrogen membrane receptor coupled to a G protein in human breast cancer cells. Endocrinology 146, 624-632.
17. Filardo, E. J., Quinn, J. A., Bland, K. I. & Frackelton, A. R., Jr. (2000). Estrogen-induced activation of Erk-1 and Erk-2 requires the G protein-coupled receptor

homolog, GPR30, and occurs via trans-activation of the epidermal growth factor receptor through release of HB-EGF. Mol Endocrinol 14, 1649-1660.
18. Filardo, E. J., Quinn, J. A., Frackelton, A. R., Jr. & Bland, K. I. (2002). Estrogen action via the G protein-coupled receptor, GPR30: stimulation of adenylyl cyclase and cAMP-mediated attenuation of the epidermal growth factor receptor-to-MAPK signaling axis. Mol Endocrinol 16, 70-84.
19. Nicole, U., Marion, L. & Michael, S. (2023). Multiplex G Protein–Coupled Receptor Screen Reveals Reliably Acting Agonists and a Gq-Phospholipase C Coupling Mode of GPR30/GPER1. Molecular Pharmacology 103, 48.
20. Prossnitz, E. R. & Barton, M. (2023). The G protein-coupled oestrogen receptor GPER in health and disease: an update. Nature Reviews Endocrinology 19, 407-424.
21. Barton, M., Filardo, E. J., Lolait, S. J., Thomas, P., Maggiolini, M. & Prossnitz, E. R. (2018). Twenty years of the G protein-coupled estrogen receptor GPER: Historical and personal perspectives. J Steroid Biochem Mol Biol 176, 4-15.
22. Vivacqua, A., Bonofiglio, D., Albanito, L., Madeo, A., Rago, V., Carpino, A., Maggiolini, M. (2006). 17beta-estradiol, genistein, and 4-hydroxytamoxifen induce the proliferation of thyroid cancer cells through the g protein-coupled receptor GPR30. Mol Pharmacol 70, 1414-1423.
23. Vivacqua, A., Bonofiglio, D., Recchia, A. G., Musti, A. M., Picard, D., Andò, S. & Maggiolini, M. (2006). The G protein-coupled receptor GPR30 mediates the proliferative effects induced by 17beta-estradiol and hydroxytamoxifen in endometrial cancer cells. Mol Endocrinol 20, 631-646.
24. Petrie, W. K., Dennis, M. K., Hu, C., Dai, D., Arterburn, J. B., Smith, H. O., Prossnitz, E. R. (2013). G protein-coupled estrogen receptor-selective ligands modulate endometrial tumor growth. Obstet Gynecol Int 2013, 472720.
25. Bologa, C. G., Revankar, C. M., Young, S. M., Edwards, B. S., Arterburn, J. B., Kiselyov, A. S., Prossnitz, E. R. (2006). Virtual and biomolecular screening converge on a selective agonist for GPR30. Nat Chem Biol 2, 207-212.
26. Pedram, A., Razandi, M. & Levin, E. R. (2006). Nature of functional estrogen receptors at the plasma membrane. Mol Endocrinol 20, 1996-2009.
27. Otto, C., Rohde-Schulz, B., Schwarz, G., Fuchs, I., Klewer, M., Brittain, D., Fritzemeier, K. H. (2008). G protein-coupled receptor 30 localizes to the endoplasmic reticulum and is not activated by estradiol. Endocrinology 149, 4846-4856.
28. Langer, G., Bader, B., Meoli, L., Isensee, J., Delbeck, M., Noppinger, P. R. & Otto, C. (2010). A critical review of fundamental controversies in the field of GPR30 research. Steroids 75, 603-610.
29. Levin, E. R. (2009). G Protein-Coupled Receptor 30: Estrogen Receptor or Collaborator? Endocrinology 150, 1563-1565.
30. Otto, C., Fuchs, I., Kauselmann, G., Kern, H., Zevnik, B., Andreasen, P., Fritzemeier, K. H. (2009). GPR30 does not mediate estrogenic responses in reproductive organs in mice. Biol Reprod 80, 34-41.
31. Kang, L., Zhang, X., Xie, Y., Tu, Y., Wang, D., Liu, Z. & Wang, Z. Y. (2010).

Involvement of estrogen receptor variant ER-alpha36, not GPR30, in nongenomic estrogen signaling. Mol Endocrinol 24, 709-721.
32. Tutzauer, J., Gonzalez de Valdivia, E., Swärd, K., Alexandrakis Eilard, I., Broselid, S., Kahn, R., Leeb-Lundberg, L. M. F. (2021). Ligand-Independent G Protein-Coupled Estrogen Receptor/G Protein-Coupled Receptor 30 Activity: Lack of Receptor-Dependent Effects of G-1 and 17β-Estradiol. Mol Pharmacol 100, 271-282.
33. Levin, E. R. & Hammes, S. R. (2016). Nuclear receptors outside the nucleus: extranuclear signalling by steroid receptors. Nature Reviews Molecular Cell Biology 17, 783-797.
34. Luo, J. & Liu, D. (2020). Does GPER Really Function as a G Protein-Coupled Estrogen Receptor in vivo? Frontiers in Endocrinology 11.
35. Seok, Y. M., Jang, E. J., Reiser, O., Hager, M. & Kim, I. K. (2012). 17β-Estradiol induces vasorelaxation in a G-protein-coupled receptor 30-independent manner. Naunyn Schmiedebergs Arch Pharmacol 385, 945-948.
36. Kim, J., Szinte, J. S., Boulware, M. I. & Frick, K. M. (2016). 17β-Estradiol and Agonism of G-protein-Coupled Estrogen Receptor Enhance Hippocampal Memory via Different Cell-Signaling Mechanisms. J Neurosci 36, 3309-3321.
37. Soltysik, K. & Czekaj, P. (2013). Membrane estrogen receptors - is it an alternative way of estrogen action? J Physiol Pharmacol 64, 129-142.
38. Razandi, M., Pedram, A., Merchenthaler, I., Greene, G. L. & Levin, E. R. (2004). Plasma membrane estrogen receptors exist and functions as dimers. Mol Endocrinol 18, 2854-2865.
39. Gingerich, S., Kim, G. L., Chalmers, J. A., Koletar, M. M., Wang, X., Wang, Y. & Belsham, D. D. (2010). Estrogen receptor alpha and G-protein coupled receptor 30 mediate the neuroprotective effects of 17β-estradiol in novel murine hippocampal cell models. Neuroscience 170, 54-66.
40. Chaudhri, R. A., Schwartz, N., Elbaradie, K., Schwartz, Z. & Boyan, B. D. (2014). Role of ERα36 in membrane-associated signaling by estrogen. Steroids 81, 74-80.
41. Li, L., Haynes, M. P. & Bender, J. R. (2003). Plasma membrane localization and function of the estrogen receptor alpha variant (ER46) in human endothelial cells. Proc Natl Acad Sci U S A 100, 4807-4812.
42. Liu, H., Zheng, Y., Wang, Y., Wang, Y., He, X., Xu, P., Xu, F. (2023). Recognition of methamphetamine and other amines by trace amine receptor TAAR1. Nature 624, 663-671.
43. Zhao, L. H., Ma, S., Sutkeviciute, I., Shen, D. D., Zhou, X. E., de Waal, P. W., Zhang, Y. (2019). Structure and dynamics of the active human parathyroid hormone receptor-1. Science 364, 148-153.
44. Liu, H., Zhang, Q., He, X., Jiang, M., Wang, S., Yan, X., Yin, W. (2023). Structural insights into ligand recognition and activation of the medium-chain fatty acid-sensing receptor GPR84. Nat Commun 14, 3271.
45. Duan, J., Xu, P., Zhang, H., Luan, X., Yang, J., He, X., Xu, H. E. (2023). Mechanism of hormone and allosteric agonist mediated activation of follicle

stimulating hormone receptor. Nat Commun 14, 519.
46. Maeda, S., Qu, Q., Robertson, M. J., Skiniotis, G. & Kobilka, B. K. (2019). Structures of the M1 and M2 muscarinic acetylcholine receptor/G-protein complexes. Science 364, 552-557.
47. Xu, P., Huang, S., Zhang, H., Mao, C., Zhou, X. E., Cheng, X., Xu, H. E. (2021). Structural insights into the lipid and ligand regulation of serotonin receptors. Nature 592, 469-473.
48. Wang, Y., Guo, S., Zhuang, Y., Yun, Y., Xu, P., He, X., Jiang, Y. (2021). Molecular recognition of an acyl-peptide hormone and activation of ghrelin receptor. Nature Communications 12, 5064.
49. Jumper, J., Evans, R., Pritzel, A., Green, T., Figurnov, M., Ronneberger, O., Hassabis, D. (2021). Highly accurate protein structure prediction with AlphaFold. Nature 596, 583-589.
50. He, X.-h., You, C.-z., Jiang, H.-l., Jiang, Y., Xu, H. E. & Cheng, X. (2023). AlphaFold2 versus experimental structures: evaluation on G protein-coupled receptors. Acta Pharmacologica Sinica 44, 1-7.
51. Kuiper, G. G., Carlsson, B., Grandien, K., Enmark, E., Häggblad, J., Nilsson, S. & Gustafsson, J. A. (1997). Comparison of the ligand binding specificity and transcript tissue distribution of estrogen receptors alpha and beta. Endocrinology 138, 863-870.
52. Xu, P., Huang, S., Zhang, H., Mao, C., Zhou, X. E., Cheng, X., Xu, H. E. (2021). Structural insights into the lipid and ligand regulation of serotonin receptors. Nature 592, 469-473.
53. Yang, F., Mao, C., Guo, L., Lin, J., Ming, Q., Xiao, P., Zhang, Y. (2020). Structural basis of GPBAR activation and bile acid recognition. Nature 587, 499-504.
54. You, C., Zhang, Y., Xu, P., Huang, S., Yin, W., Eric Xu, H. & Jiang, Y. (2022). Structural insights into the peptide selectivity and activation of human neuromedin U receptors. Nature Communications 13, 2045.
55. Wu, H., Wacker, D., Mileni, M., Katritch, V., Han, G. W., Vardy, E., Stevens, R. C. (2012). Structure of the human κ-opioid receptor in complex with JDTic. Nature 485, 327-332.
56. Wang, Y., Zhuang, Y., DiBerto, J. F., Zhou, X. E., Schmitz, G. P., Yuan, Q., Xu, H. E. (2023). Structures of the entire human opioid receptor family. Cell 186, 413-427.e417.
57. Liu, Q., Yang, D., Zhuang, Y., Croll, T. I., Cai, X., Dai, A., Jiang, Y. (2021). Ligand recognition and G-protein coupling selectivity of cholecystokinin A receptor. Nature Chemical Biology 17, 1238-1244.

Methods

Cell lines

Spodoptera frugiperda (Sf9, Expression systems) and *Trichoplusia ni.* (High Five, Thermo Fisher) cells were grown in ESF 921 medium at 27°C and 120 rpm. HEK293T cells were grown in a humidified 37°C incubator with 5% CO2 using media supplemented with 100 I.U./mL penicillin and 100 mg/mL streptomycin (Invitrogen). The human cell lines HEK293T were maintained in DMEM (VWR) containing 10% fetal bovine serum (FBS, VWR).

Plasmids construct

For structure determination of the E2, G1, fulvestrant and apo GPR30-Gq complex, the full-length gene sequence of wild-type human GPR30 was cloned into pFastBac vector with an N-terminal HA signaling peptide sequence followed by a FLAG tag, a 10×His tag and a BRIL to facilitate expression and purification[58]. The engineered Gαq (hereafter Gαq) construct was generated based on mini-Gs/q713, which carries two dominant-negative mutations (corresponding to G203A and A326S) to decrease the affinity of nucleotide-binding and facilitate the stability of Gαβγ complex[59]. The N terminal 1–18 amino acids and the α-helical domain of the mini-Gs/q71 were substituted by the corresponding sequences of the human Gαi1 contributing to binding to the antibody fragments scFv16[60]. All the three G protein complex components, Gαq, rat Gβ1 and bovine Gγ2, were cloned into pFastBac vector separately. For structure determination of the Lys05 stimulated GPR30-Gq complex, the engineered Gαq was fused to the C-terminus of GPR30 with flexible linker between them. Gβ1 and Gγ2 were cloned into a pFastBac Dual vector.

Complex expression and purification

The complexes are all expressed in Hi5 insect cells (Invitrogen). For expression of E2, G1 and fulvestrant stimulated GPR30-Gq complex, and apo-GPR30-Gq complex, cell cultures were grown in ESF 921 medium (Expression system) to a density of 3×10^6 per

mL with virus preparations for GPR30, Gαq, Gβ1, Gγ2, and scFv16 at the ratio of 1:1:1:1:1. For expression of Lys05 activated GPR30-Gq complex, cell cultures were grown to a density of 3×10^6 per mL with two separate virus preparations for GPR30-Gαq and Gβ1γ2 at a ratio of 1:1.2. The infected cells were cultured at 27°C for 48 h before collection by centrifugation and the cell pellets were stored at -80°C.

For the purification of the E2, G1 and fulvestrant stimulated GPR30-Gq complex, cell pellets from 1 L culture were thawed at room temperature and resuspended in low salt buffer containing 20 mM HEPES pH 7.4, 100 mM NaCl, 5 mM $CaCl_2$, 5 mM $MgCl_2$, 10% glycerol, protease inhibitor cocktail (Thermo Fisher Scientific). The GPR30-Gq complexes were formed on membrane in the presence of 1 μM E2 or 1 μM G1 (Targetmol.USA) or 1 μM fulvestrant (Sigma), and treated with apyrase (20 mU mL-1, NEB), followed by incubation 1 hour at 4℃. Subsequently, 0.5% (w/v) n-dodecyl-β-d-maltoside (DDM, Anatrace) and 0.1% (w/v) cholesteryl hemisuccinate (CHS, Anatrace) were added to solubilize complexes for 2-3 h at 4°C. Insoluble materials was removed by centrifugation at 30,000 g for 30 min and the supernatant was immobilized by batch binding to Talon affinity resin. After batch binding, the TALON IMAC resin with immobilized protein complex was manually loaded onto a gravity flow column. The TALON IMAC resin was washed with 10 column volumes of 20 mM HEPES, pH 7.4, 100 mM NaCl, 5 mM $CaCl_2$, 5 mM $MgCl_2$, 30 mM imidazole, 10% glycerol, 0.1% LMNG (w/v), 0.02% CHS (w/v), 1 μM E2 or 1 μM G1 or 1 μM fulvestrant and eluted with the same buffer plus 250 mM imidazole, 1 μM E2 or 1 μM G1 or 1 μM fulvestrant. The mixture was then purified by SEC using a Superdex 200 10/300 GL column (GE healthcare) in 20 mM HEPES, pH 7.4, 100 mM NaCl, 0.00075% (w/v) LMNG, 0.00025% (w/v) GDN and 1 μM E2 or 1 μM G1 or 1 μM fulvestrant. For the purification of apo-GPR30-Gq complex, all steps are same as aforementioned without ligand added. For the purification of the Lys05 stimulated GPR30-Gq complex, 500 μM Lys05 (Targetmol.USA) was added throughout the purification, and the eluted protein was incubated with 20 μg/mL of Nb35 at 4 °C for another 1 h. The mixture was then purified

by SEC using a Superdex 200 10/300 GL column (GE healthcare) in 20 mM HEPES, pH 7.4, 100 mM NaCl, 0.00075% (w/v) LMNG, 0.00025% (w/v) GDN and 500 μM Lys05. All sample are finally concentrated to ~8 mg/mL for cryo-EM grids preparation

Cryo-EM grid preparation and data collection

For cryo-EM grids preparation of the GPR30-Gq complexes, 3 μL of the protein at ~8 mg/mL were loaded onto a glow-discharged holey carbon grid (Quantifoil Au 300 mesh R1.2/1.3), and subsequently were plunge-frozen in liquid ethane using Vitrobot Mark IV (Thermo Fischer Scientific). The data of E2, G1 and fulvestrant stimulated GPR30-Gq complex were collected at the electron microscopy facility of Shanghai Institute of Materia Medica (SIMM) on a Titan Krios at 300 kV using Gatan K3 Summit detector with a pixel size of 1.071 Å at the Shanghai Institute of Materia Medica, Chinese Academy of Sciences. Images were taken at a dose rate of about 8.0 e/Å2/s with a defocus ranging from -1.0 to -2.0 μm using the Serial-EM software[61]. The total exposure time was 8 s, and 36 frames were recorded per micrograph. A total of 4,773, 4,840 and 7,980 movies were collected for E2, G1 and fulvestrant stimulated GPR30-Gq complex, respectively.

For apo GPR30-Gq complex, cryo-EM imaging was collected on a Titan Krios at 300 kV using Gatan K3 Summit detector with a pixel size of 0.824 Å at the Shanghai Advanced Center for Electron Microscopy, Shanghai Institute of Materia Medica, Chinese Academy of Sciences. Images were taken at a dose rate of about 8.0 e/Å2/s with a defocus ranging from -1.0 to -2.0 μm using the EPU software (FEI Eindhoven, Netherlands). The total exposure time was 8 s, and 36 frames were recorded per micrograph. A total of 6,691 movies were collected.

For Lys05 activated GPR30-Gq complex, Cryo-EM imaging was collected on a Titan Krios equipped with a Falcon 4 direct electron detection device at 300 kV. Images were taken with a pixel size of 0.73 Å, a defocus ranging from -1.0 to -2.0 μm using the EPU

software (FEI Eindhoven, Netherlands). We collected a total of 9,417 movies with total dose of 50 e/Å2/s over 2.5 s exposure on each EER format movie. Each movie was divided into 36 frames during motion correction.

Image processing and map construction

For the dataset of the E2 stimulated GPR30-Gq complex, image stacks were subjected to beam-induced motion correction using MotionCor2[62]. Contrast transfer function (CTF) parameters for each non-dose-weighted micrograph were determined by Gctf[63]. Automated particle selection and data processing were performed using RELION-3.0 beta2[64]. Automated yielded particles were extracted on a binned dataset with a pixel size of 2.142 Å and were subjected to reference-free 2D classification, producing 1,199,129 particles with well-defined averages. Further 3D classification produced two good subsets showing clear structural features accounting for 527,631 particles. These particles were re-extracted into a pixel of 1.071 and subsequently subjected to CTF refinement, Bayesian polishing. Further 3D classifications with no alignment produced a high-quality subsets accounting for 177,591 particles. 3D refinement and post process generated a map with an indicated global resolution of 3.2 Å at a Fourier shell correlation (FSC) of 0.143.

For the dataset of the fulvestrant stimulated GPR30-Gq complex, image stacks were subjected to beam-induced motion correction using MotionCor2[62]. CTF parameters for each non-dose-weighted micrograph were determined by Gctf[63]. Automated yielded particles were extracted on a binned dataset with a pixel size of 2.142 Å and were subjected to reference-free 2D classification, producing 3,410,733 particles with well-defined averages. Further 3D classification produced a good subset showing clear structural features accounting for 826,321 particles. These particles were re-extracted into a pixel of 1.071 and subsequently subjected to 3D classifications with no alignment produced a high-quality subsets accounting for 536,691 particles. 3D refinement and

post process generated a map with an indicated global resolution of 3.2 Å at a FSC of 0.143.

For the dataset of the G1 stimulated GPR30-Gq complex, image stacks were subjected to beam-induced motion correction using MotionCor2[62]. CTF parameters for each non-dose-weighted micrograph were determined by Gctf[63]. Automated particle selection and data processing were performed using RELION-3.0 beta2[64]. Automated yielded and subsequent reference-free 2D classification produced 1,065,934 well-defined particles were imported into cryoSPARC.v4[65]. Further ab-initio model and heterogeneous refinement followed by a resolution ladder hetero-refinement produced a high-quality subset accounting for 411,141 particles. The Non-uniform refinement generated a map with an indicated global resolution of 3.1 Å at a FSC of 0.143.

For the dataset of the apo-GPR30-Gq complex, the single particle analysis was performed with cryoSPARC.v4[65]. Dose-fractionated image stacks were subjected to motion correction by MotionCor2[62]. CTF parameters for micrograph were estimated by patch CTF estimation. The auto-picked particles were extracted and subjected to reference-free 2D classification. The selected 1,072,840 particles were subjected to ab-initio model and heterogeneous refinement, produced a high-quality subset accounting for 345,373 particles. Further ab-initio model and heterogeneous refinement produced a subset of 300,561 particles for Non-uniform refinement and generated a map with an indicated global resolution of 2.9 Å at a FSC of 0.143.

For the dataset of the Lys05 activated GPR30-Gq complex, the single particle analysis was performed with cryoSPARC.v4[65]. Dose-fractionated image stacks were subjected to motion correction by MotionCor2[62]. CTF parameters for micrograph were estimated by patch CTF estimation. The auto-picked particles were extracted and subjected to reference-free 2D classification. The selected 1,457,109 particles were subjected to ab-initio model and heterogeneous refinement, produced a high-quality subset accounting

for 274,405 particles. Further ab-initio model and heterogeneous refinement produced a subset of 209,371 particles for Non-uniform refinement and generated a map with an indicated global resolution of 2.6 Å at a FSC of 0.143.

Model building and refinement

Predicted model of active-state GPR30 receptor from AlphaFold[49] were used as initial model for rebuilding and refinement against the electron microscopy density map. UCSF Chimera-1.14[66] was used to dock the model into the electron microscopy density map, and followed by iterative manual adjustment and rebuilding in COOT-0.9.6[67] and ISOLDE-1.2[68]. Then models were further refined and validated in Phenix-1.20 programs[69] (Table S1). Structural figures were generated using UCSF Chimera-1.14[66], ChimeraX-1.2[70] and PyMOL-2.0 (https://pymol.org/2/).

Cell transfection

The Wild type GPR30 gene was subcloned into pcDNA3.0 vector with the addition of an N-terminal HA tag. All the mutations used for functional studies were generated by QuickChange PCR and were verified by DNA sequencing. HEK293 cells were obtained from ATCC (Manassas, VA, USA) and cultured in DMEM supplemented with 10% (v/v) FBS, 100 mg/L penicillin, and 100 mg/L streptomycin in 5% CO_2 at 37°C. For transient transfection, approximately 2×10^6 cells were mixed with plasmids in 200 μL transfection buffer, and electroporation was carried out with a Scientz-2C electroporation apparatus (Scientz Biotech, Ningbo, China). The experiments were carried out 24 h after transfection.

Surface expression analysis

24 hours after transfection, cells were washed with PBS, fixed with 4% PFA for 15 min, and then blocked with 2% BSA for 1 h. Next, cells were incubated with the polyclonal anti-HA (Sigma, H6908) overnight at 4°C and then horseradish peroxidase (HRP)-conjugated anti-rabbit antibody (CST, 7074S) for 1 h at room temperature. Then cells were washed and incubated with 50 μL tetramethylbenzidine (Sigma, T0440) for 30

min before the reaction was stopped with 25 μL TMB Substrate stop solution (Beyotime, P0215). Absorbance at 450 nm was quantified using a FlexStation III microplate reader (Molecular Devices).

IP1 accumulation assay

IP1 accumulation was measured using the IP-ONE Gq HTRF kit (Cisbio, 621PAPEJ). Briefly, 24 hours after transfection, cells were harvested and resuspended in DMEM containing 0.1% BSA at a density of 4 million per milliliter. 5 ml cells were aliquoted into 384-well plate and stimulated with 5 ml compounds in DMEM (0.1% BSA) supplemented with 50 mM LiCl. After incubation at 37 °C for 30 minutes, 5 ml IP1 d2 reagent and 5 ml IP1 Tb cryptate antibody were added. After incubation at room temperature for another 1 h, HTRF was read on EnVision multiplate reader (PerkinElmer). EC_{50} values for each curve were calculated by Prism 8.0 software (GraphPad Software).

Calcium assay

Cells were seeded in 96-well plates at a density of 3×10^4 cells/well and cultured overnight. The cells were then incubated with 2 μmol/L Fluo-4 AM in HBSS (5.4 mmol/L KCl, 0.3 mmol/L Na_2HPO_4, 0.4 mmol/L KH_2PO_4, 4.2 mmol/L $NaHCO_3$, 1.3 mmol/L $CaCl_2$, 0.5 mmol/L $MgCl_2$, 0.6 mmol/L $MgSO_4$, 137 mmol/L NaCl, 5.6 mmol/L D-glucose and 250 μmol/L sulfinpyrazone, pH 7.4) at 37 °C for 40 min. After a thorough washing, 50 μL of HBSS was added. After incubation at room temperature for 10 min, 25 μL of agonist was dispensed into the well using a FlexStation III microplate reader (Molecular Devices), and the intracellular calcium change was recorded at an excitation wavelength of 485 nm and an emission wavelength of 525 nm. EC_{50} and Emax values for each curve were calculated by Prism 8.0 software (GraphPad Software).

cAMP accumulation assay

cAMP accumulation was measured using the cAMP kit (PerkinElmer, TRF0264). Briefly, 24 hours after transfection, cells were harvested and resuspended in DMEM containing 0.1% BSA at a density of 2×10^5 cells/mL. Cells were then plated onto 384-well assay plates at 1000 cells/5 μL/well. To test the Gs activity of compounds on GPR30, another 5 μL buffer containing compounds with 500 μM IBMX were added to the cells. To test the Gi activity of compounds on GPR30, 5 μlL buffer containing compounds with 1 μM forskolin and 500 μM IBMX were added to the cells. After incubation at 37 °C for 30 minutes, intracellular cAMP level was tested by a LANCE Ultra cAMP kit and EnVision multiplate reader according to the manufacturer's instructions. EC_{50} values for each curve were calculated by Prism 8.0 software (GraphPad Software).

Ligand Binding assay

CV1 cells were cultured in DMEM medium with 10% FBS and seeded at a density of 30,000 cells/well in Isoplate-96 plates (PerkinElmer). Twenty-four hours after transfection with the GPR30 or ERα, CV1 cells were washed twice and incubated with blocking buffer (DMEM supplemented with 25 mM HEPES and 0.1% (w/v) BSA, pH 7.4) for 2 h at 37°C. For homogeneous competition binding, radiolabeled [^{3}H]-E2 (PerkinElmer, 3 nM) and unlabeled compound at seven decreasing concentrations (Estradiol, G-1, Tamoxifen, Raloxifene, 10 μM to 1 pM) were added and competitively reacted with the cells in blocking buffer at RT for 3 h. Following incubation, cells were washed three times with ice-cold PBS and lysed by 50 μL lysis buffer (PBS supplemented with 20 mM Tris-HCl, 1% Triton X-100, pH 7.4). The radioactivity was subsequently counted (counts per minute, CPM) in a scintillation counter (MicroBeta 2 Plate Counter, PerkinElmer) using a scintillation cocktail (OptiPhase SuperMix, PerkinElmer). Data were analyzed by nonlinear regression using GraphPad Prism 8.0 software.

Hi5 cell binding assays were carried out in filter plates. Hi5 membrane homogenates expressing ERα or GPR30 (10 μg protein per well) were incubated in membrane binding buffer (20 mM HEPES-NaOH and 10 mM EDTA, pH 7.4) with 50 nM [^{3}H]-E2 at room temperature for 3 h. Following incubation, the samples were filtered rapidly in vacuum through glass fiber filter plates (PerkinElmer). After soaking and rinsing 4 times with ice-cold PBS, the filters were dried before the addition of 50 μL of scintillation cocktail (PerkinElmer) and counted for radioactivity in a scintillation counter (PerkinElmer). Data were analyzed by GraphPad Prism 8.0 software.

References

58. Chun, E., Thompson, A. A., Liu, W., Roth, C. B., Griffith, M. T., Katritch, V., Stevens, R. C. (2012). Fusion partner toolchest for the stabilization and crystallization of G protein-coupled receptors. Structure 20, 967-976.
59. Liu, P., Jia, M. Z., Zhou, X. E., De Waal, P. W., Dickson, B. M., Liu, B., Jiang, Y. (2016). The structural basis of the dominant negative phenotype of the Gαi1β1γ2 G203A/A326S heterotrimer. Acta Pharmacol Sin 37, 1259-1272.
60. Maeda, S., Koehl, A., Matile, H., Hu, H., Hilger, D., Schertler, G. F. X., Kobilka, B. K. (2018). Development of an antibody fragment that stabilizes GPCR/G-protein complexes. Nat Commun 9, 3712.
61. Mastronarde, D. N. (2005). Automated electron microscope tomography using robust prediction of specimen movements. J Struct Biol 152, 36-51.
62. Zheng, S. Q., Palovcak, E., Armache, J. P., Verba, K. A., Cheng, Y. & Agard, D. A. (2017). MotionCor2: anisotropic correction of beam-induced motion for improved cryo-electron microscopy. Nat Methods 14, 331-332.
63. Zhang, K. (2016). Gctf: Real-time CTF determination and correction. J Struct Biol 193, 1-12.
64. Scheres, S. H. (2012). RELION: implementation of a Bayesian approach to cryo-EM structure determination. J Struct Biol 180, 519-530.
65. Punjani, A., Rubinstein, J. L., Fleet, D. J. & Brubaker, M. A. (2017). cryoSPARC: algorithms for rapid unsupervised cryo-EM structure determination. Nat Methods 14, 290-296.
66. Pettersen, E. F., Goddard, T. D., Huang, C. C., Couch, G. S., Greenblatt, D. M., Meng, E. C. & Ferrin, T. E. (2004). UCSF Chimera--a visualization system for exploratory research and analysis. J Comput Chem 25, 1605-1612.
67. Emsley, P. & Cowtan, K. (2004). Coot: model-building tools for molecular graphics. Acta Crystallogr D Biol Crystallogr 60, 2126-2132.
68. Croll, T. I. (2018). ISOLDE: a physically realistic environment for model building into low-resolution electron-density maps. Acta Crystallogr D Struct Biol 74, 519-530.
69. Adams, P. D., Afonine, P. V., Bunkóczi, G., Chen, V. B., Davis, I. W., Echols, N., Zwart, P. H. (2010). PHENIX: a comprehensive Python-based system for macromolecular structure solution. Acta Crystallogr D Biol Crystallogr 66, 213-221.
70. Pettersen, E. F., Goddard, T. D., Huang, C. C., Meng, E. C., Couch, G. S., Croll, T. I., Ferrin, T. E. (2021). UCSF ChimeraX: Structure visualization for researchers, educators, and developers. Protein Sci 30, 70-82.

Fig. 1

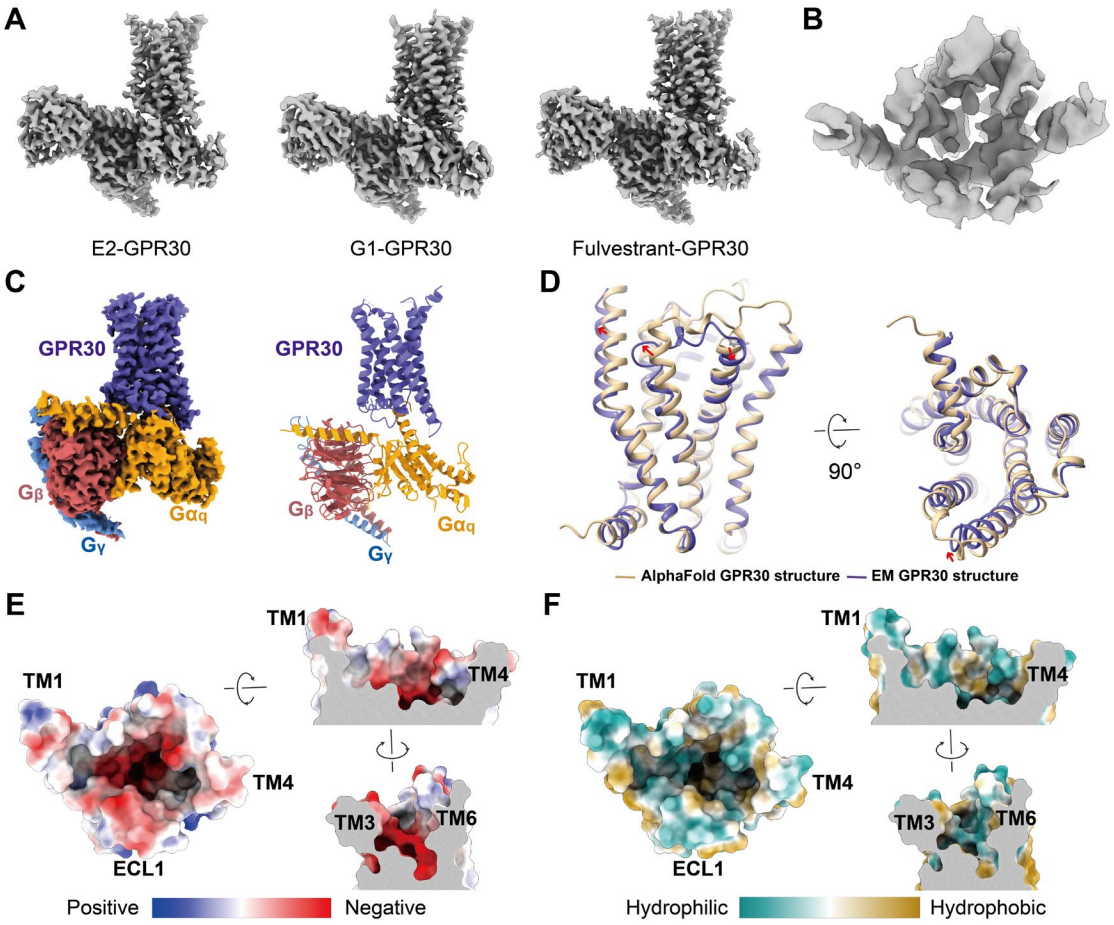

Figure 1. Cryo-EM structures contradict GPR30 as a direct estrogen receptor.

(A) Cryo-EM maps of GPR30-Gq structures in the presence E2, G-1, and fulvestrant.

(B) No ligand density observed in the GPR30 binding pocket.

(C) Cryo-EM density map and cartoon presentation of the apo-GPR30-Gq complex.

(D) Comparison of the EM GPR30 structure with the AlphaFold predicted GPR30 structure.

(E-F) Negatively charged (E) and hydrophilic (F) nature of GPR30's binding pocket.

Fig. 2

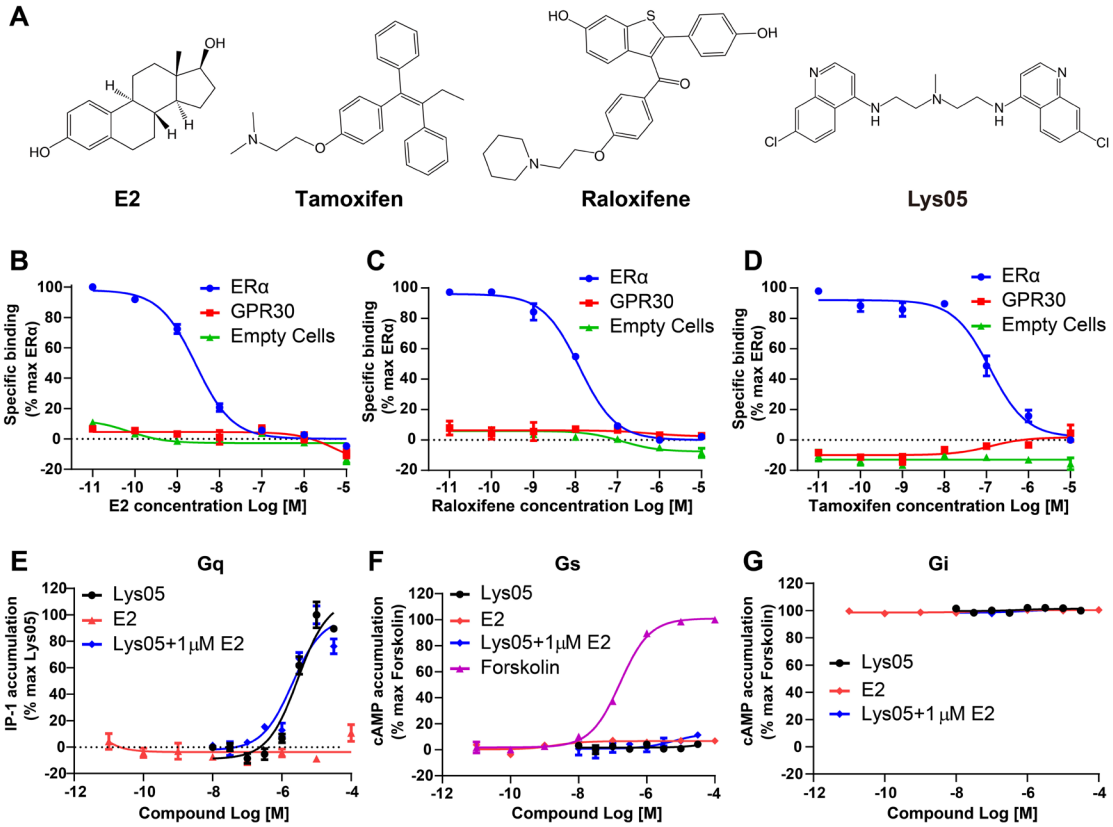

Figure 2. Functional assays challenge GPR30 as a direct estrogen receptor.

(A) Chemical formula of E2, tamoxifen, raloxifene and Lys05.

(B-D) Radioligand competitive binding results of E2 (B), tamoxifen (C), or raloxifene (D) to GPR30, ERα and empty cell. Data are mean ± S.E.M. from 3 independent experiments (n = 3).

(E-G) Cell-based functional assays to evaluate stimulation of E2, Lys05, or E2+Lys05 for Gq (E), Gs (F), or Gi (G) pathways. Data are mean ± S.E.M. from 3 independent experiments (n = 3).

Fig. 3

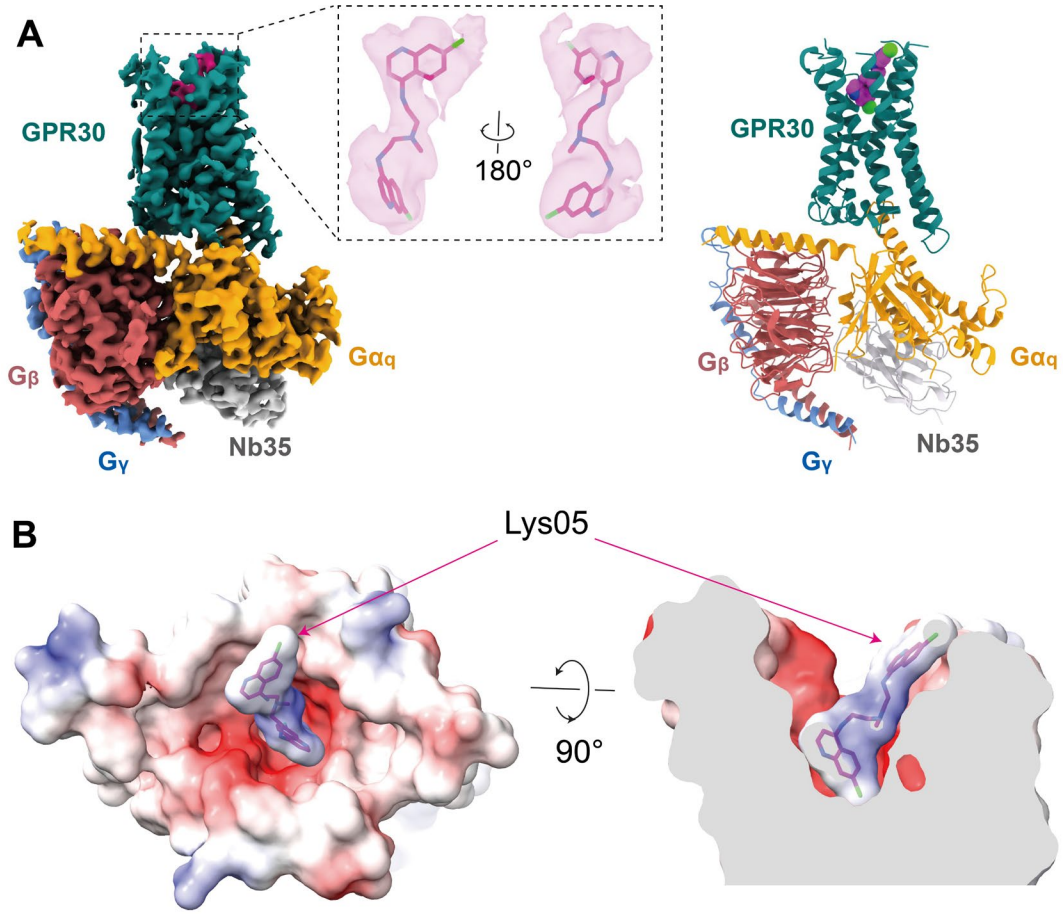

Figure 3. Structure of GPR30 bound to Lys05.

(A) Cryo-EM density map and cartoon presentation of the Lys05-GPR30-Gq complex. The complex density map is shown at a contour level of 0.15.

(B) Positively charged Lys05 accommodated in the negatively charged ligand binding pocket of GPR30.

Fig. 4

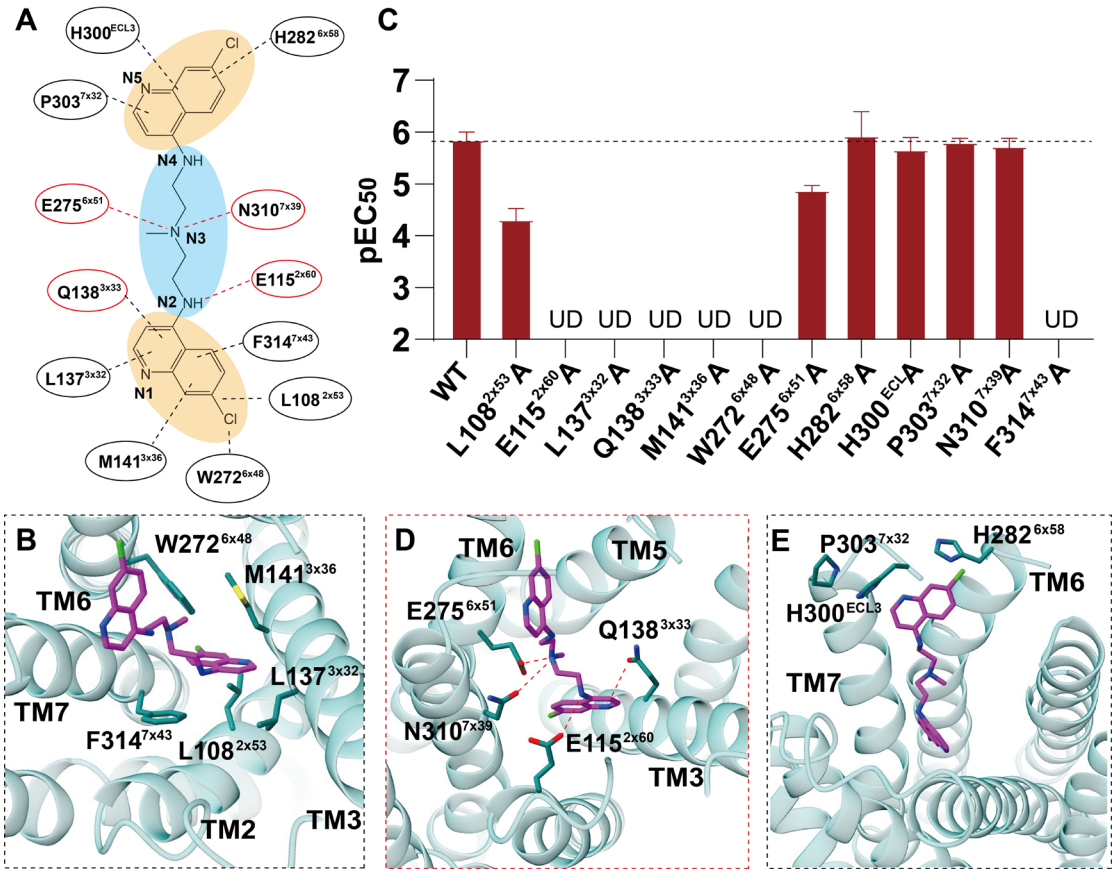

Figure 4. Molecular Recognition of Lys05 by GPR30.

(A) Diagram of Lys05 interacting residues, the background indicated two hydrophobic (orange) and one hydrophilic (light blue) moieties of Lys05. The residues and dotted line in red color represent polar nature or interactions, and that in black represent hydrophobic nature or interactions.

(B, D, E) Detailed interactions of the tri-layered interface between Lys05 and GPR30, the bottom hydrophobic interactions (B), the center hydrophilic interactions (D), and the top hydrophobic interactions (E).

(C) Effects of mutating GPR30-Lys05 interacting residues within the ligand binding pocket. The pEC_{50} is shown in the Bar graph. Data are mean ± S.E.M. from 3 independent experiments (n = 3).

Fig. 5

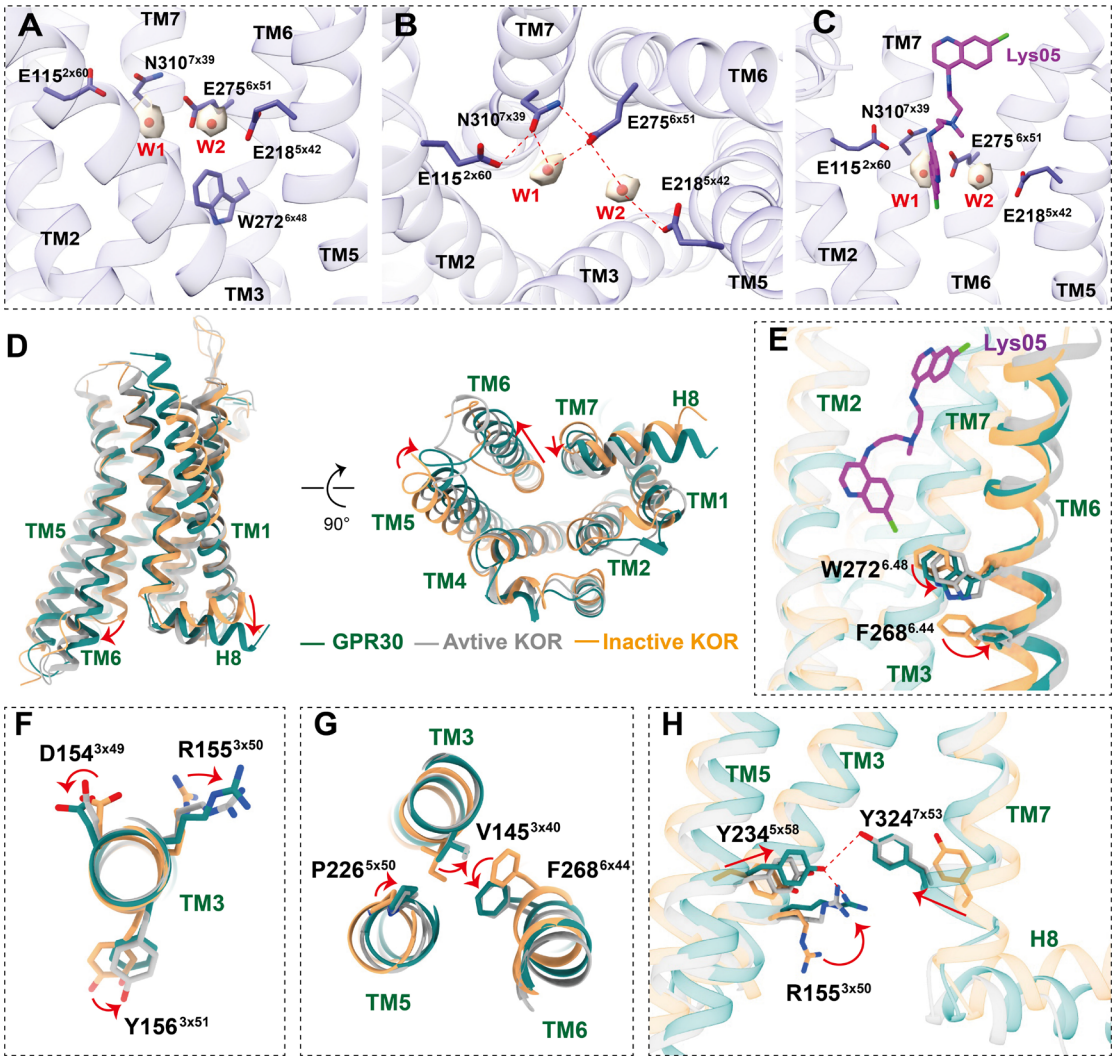

Figure 5. Basal activity and ligand-induced activation of GPR30.

(A-B) Side view (A) and top view (B) of water molecules and surrounding residues in the apo-GPR30-Gq structure pocket.

(C) Superposition of Lys05 and water molecules in the structures of the GPR30-Gq complexes.

(D) Superposition of activated GPR30 (cornflower blue) with active KOR (gray; PDB code: 8F7W) and inactive KOR (orange; PDB code: 4DJH). Notable conformational changes occur at intracellular ends of TM6 and TM7 upon receptor activation, side view (left) and bottom view (right).

(E) The "switch" W272^{6x48} of GPR30 display relative rotameric change when sensing

Lys05 and further induced conformational change of F268^{6x44}.

(F-H) The key D-R155^{3x50}-Y motif (F), P-V145^{3x40} – F268^{6x44} (G) and N-P^{7x50}-xx-Y324^{7x53} (H) motifs displayed conformational rearrangement in activated GPR30.

Fig. 6

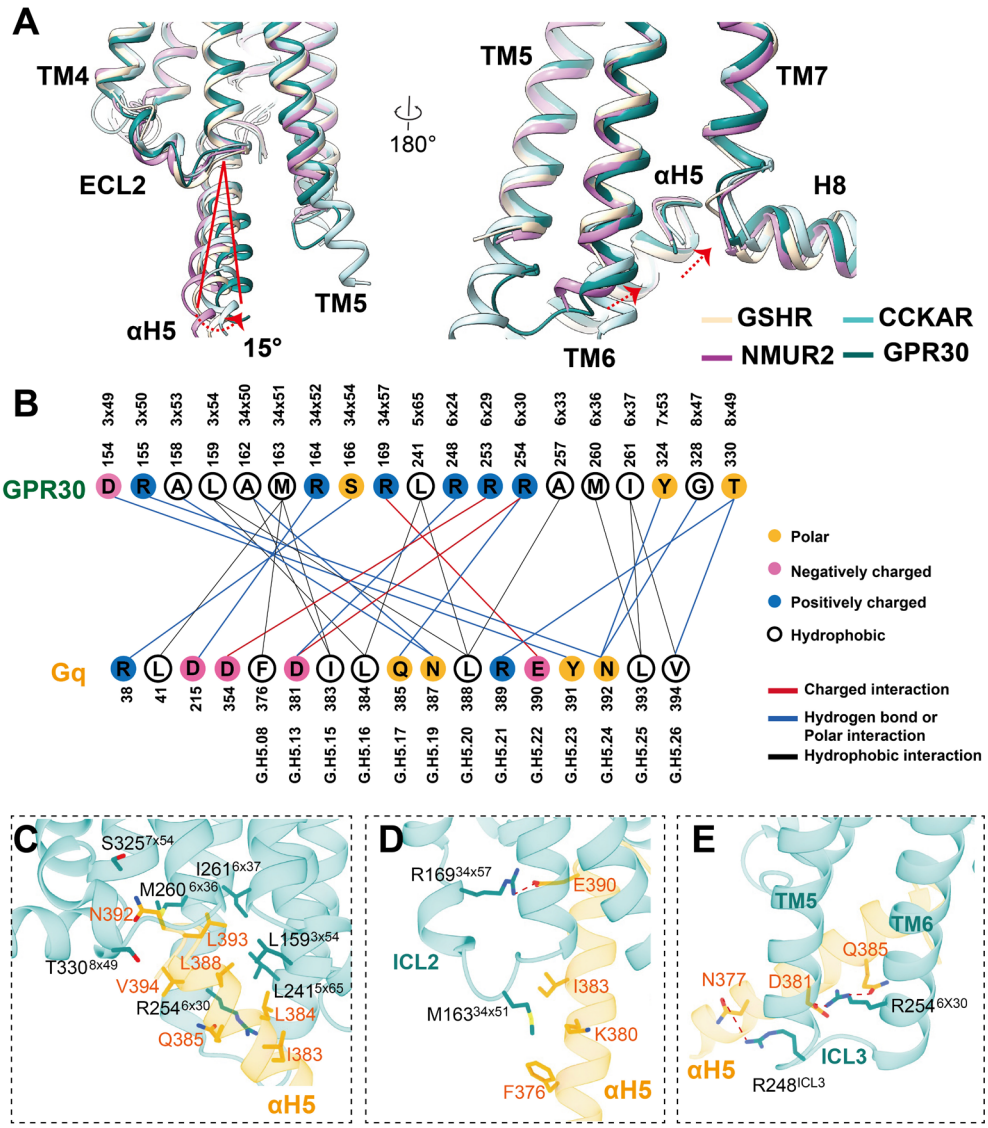

Fig. 6 Gαq coupling of GPR30.

(A) Compared to GSHR (PDB code: 7F9Z), CCKAR (PDB code: 7EZM) and NMUR2 (PDB code: 7W55), the N-terminus of αH5 is positioned closer to the junction of TM5 and TM6 in GPR30, diverging by approximately 15°.

(B) Diagram of the GPR30 - Gαq contacts.

(C) Key interactions between the TMs that forms the core cavity for Gq coupling and αH5 of Gαq.

(D-E) Key interactions between the ICL2 (D) and ICL3 (E) from GPR30and αH5 of Gαq.

Fig. S1

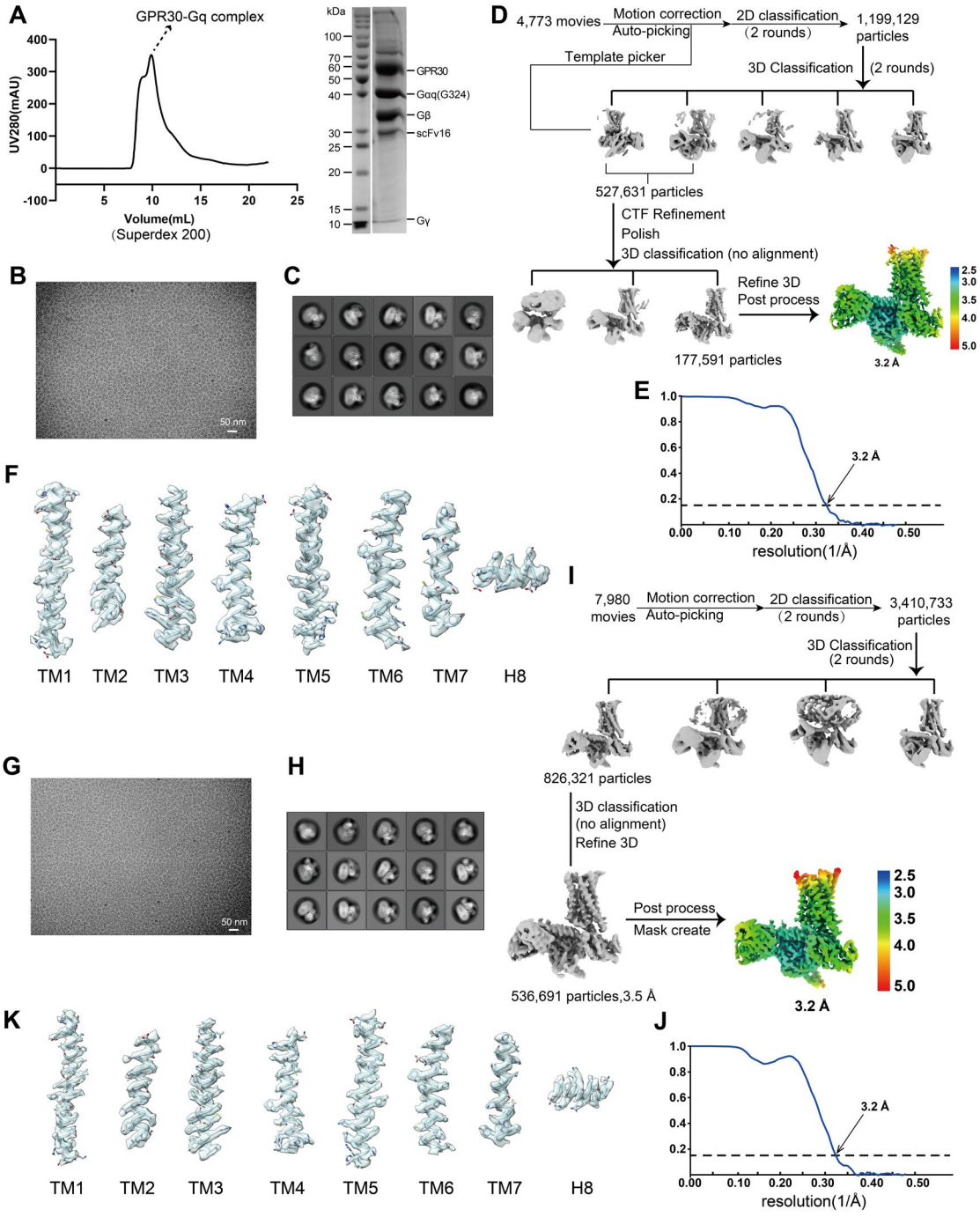

Fig. S1 Purification and structure determination of GPR30-Gq complexes in the presence of E2 and fulvestrant.

(A) Representative size exclusion chromatography (SEC) profiles and SDS-PAGE analysis of GPR30-Gq complex.

(B-C) Representative cryo-EM image (B) and 2D classification averages (C) of GPR30-

Gq complex in the presence of E2.

(D-E) Cryo-EM data processing flowcharts (D) and the Fourier shell correlation (FSC) curves (E) of GPR30-Gq complex in the presence of E2. The global resolution of the final processed density map estimated at the FSC = 0.143 is 3.2 Å.

(F) The density maps of TM1–TM7 and helix 8(H8) of GPR30 in GPR30-Gq complex in the presence of E2.

(G-H) Representative cryo-EM image (G) and 2D classification averages (H) of GPR30-Gq complex in the presence of fulvestrant.

(I-J) Cryo-EM data processing flowcharts (I) and the Fourier shell correlation (FSC) curves (J) of GPR30-Gq complex in the presence of fulvestrant. The global resolution of the final processed density map estimated at the FSC = 0.143 is 3.2 Å.

(K) The density maps of TM1–TM7 and helix 8(H8) of GPR30 in GPR30-Gq complex in the presence of fulvestrant.

Fig. S2

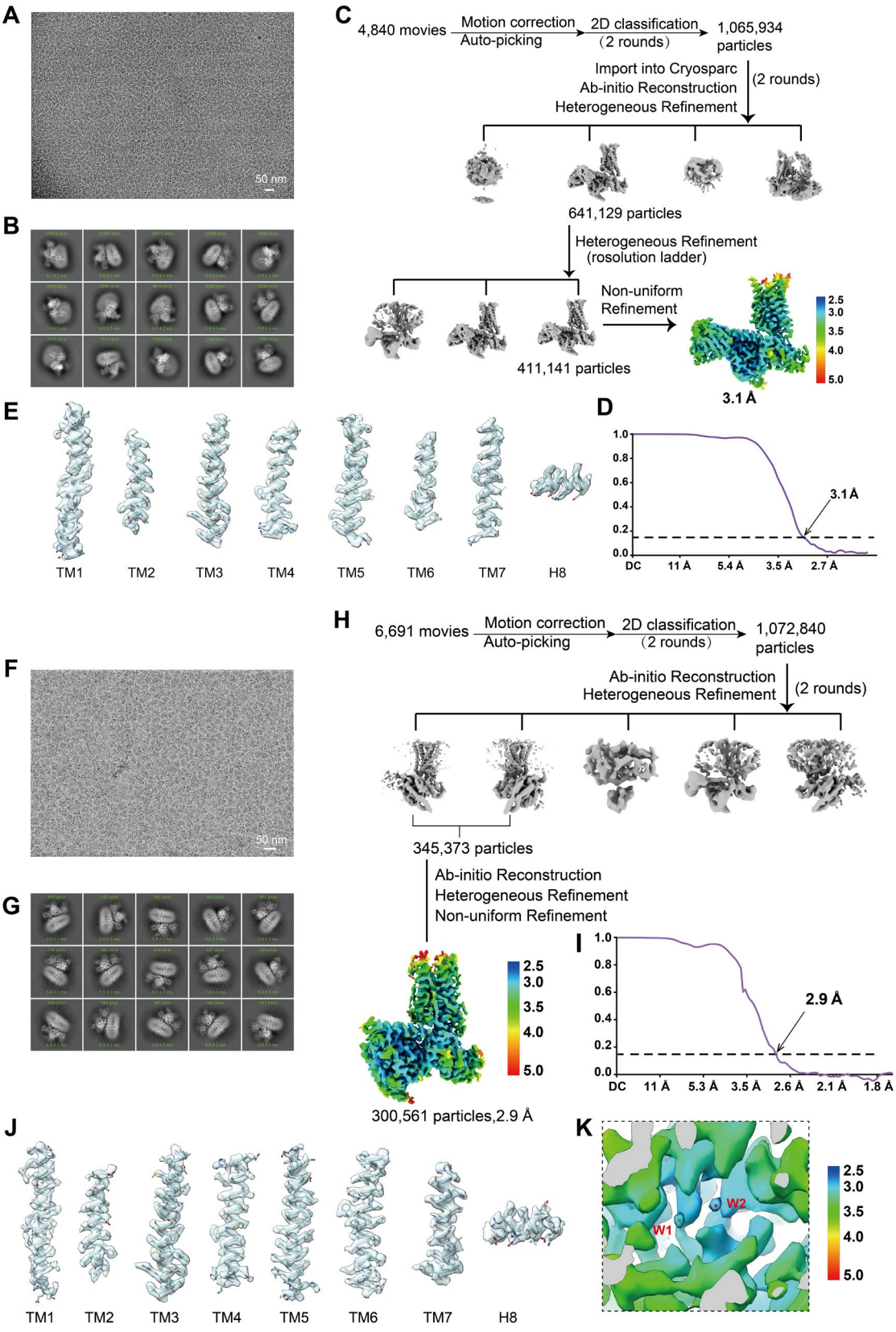

Fig. S2 Purification and structure determination of GPR30-Gq complexes in the

presence of G1 and apo- GPR30-Gq complexes.

(A-B) Representative cryo-EM image (A) and 2D classification averages (B) of GPR30-Gq complex in the presence of G1.

(C-D) Cryo-EM data processing flowcharts (C) and the Fourier shell correlation (FSC) curves (D) of GPR30-Gq complex in the presence of G1. The global resolution of the final processed density map estimated at the FSC = 0.143 is 3.1 Å.

(E) The density maps of TM1–TM7 and helix 8(H8) of GPR30 in GPR30-Gq complex in the presence of G1.

(F-G) Representative cryo-EM image (F) and 2D classification averages (G) of apo-GPR30-Gq complex.

(H-I) Cryo-EM data processing flowcharts (H) and the Fourier shell correlation (FSC) curves (I) of apo-GPR30-Gq complex. The global resolution of the final processed density map estimated at the FSC = 0.143 is 2.9 Å.

(J) The density maps of TM1–TM7 and helix 8(H8) of GPR30 in apo-GPR30-Gq complex.

(K) Local resolution for the density of water molecules (W1–W2) in the ligand-binding pocket of the apo-GPR30-Gq structure.

Fig. S3

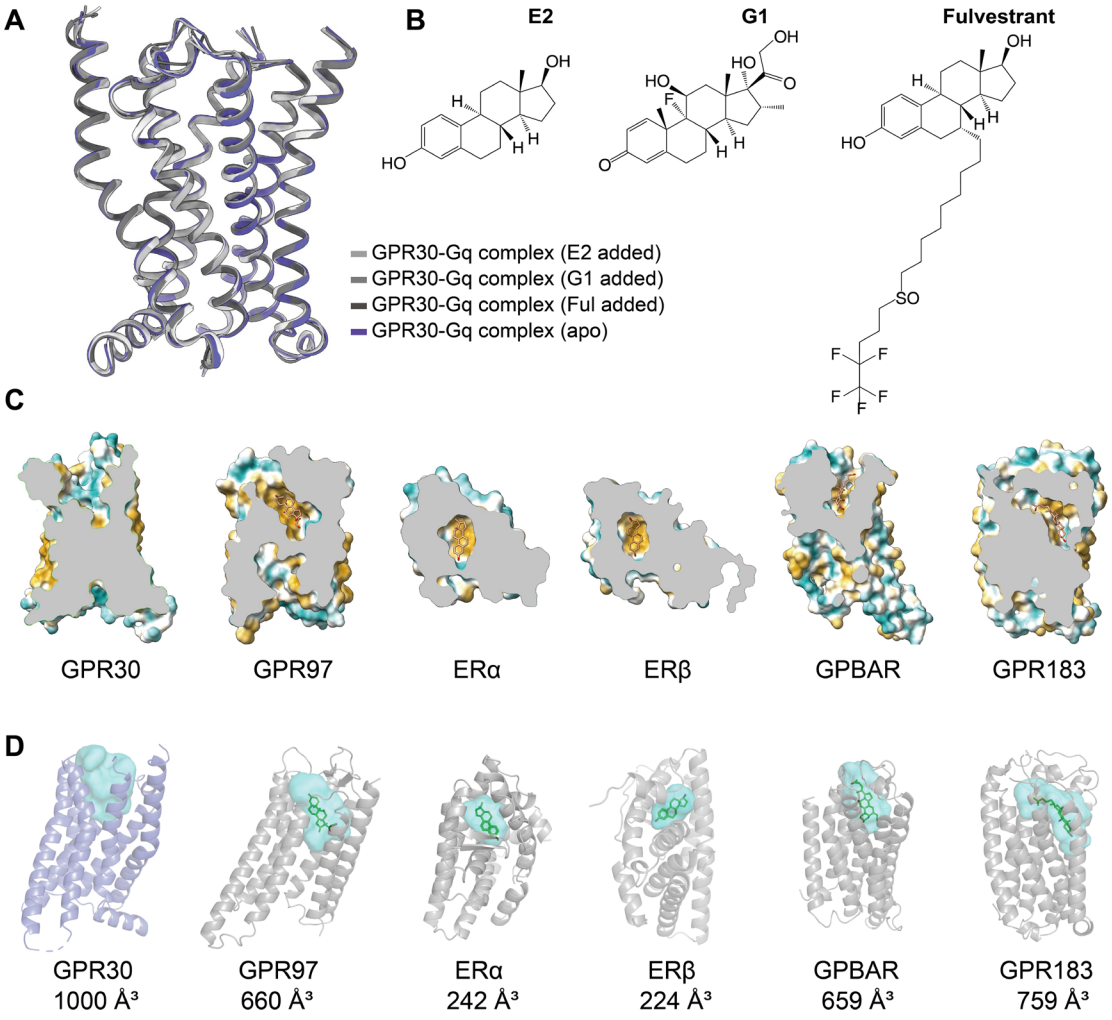

Fig. S3 Comparisons of GPR30 structures, and the difference between GPR30's binding pocket and that of related steroid hormone receptors

(A) Comparisons of GPR30 structures.

(B) Chemical formula of hydrophobic ligand E2, G1 and fulvestrant.

(C-D) The hydrophilic nature and larger volume of the GPR30 pocket is in contrast to that of the related steroid hormone receptors.

Fig. S4

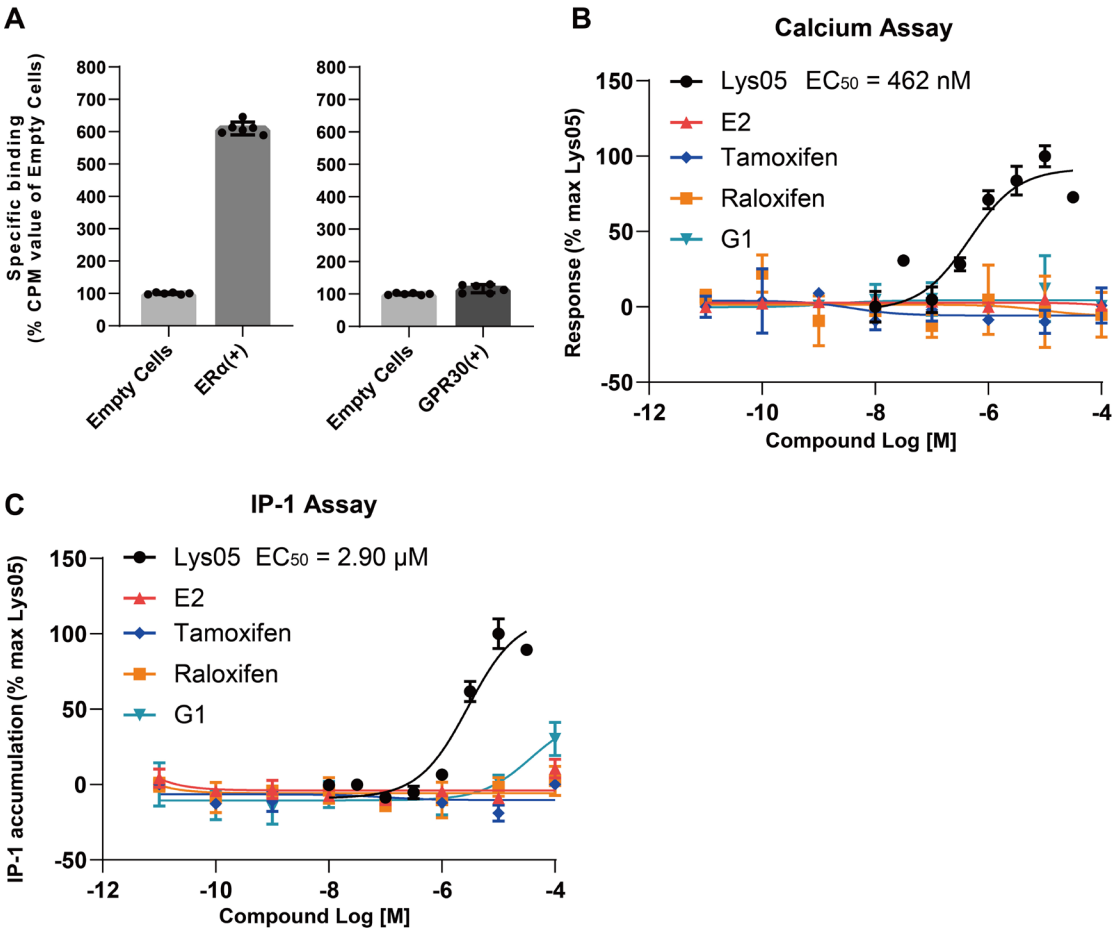

Fig. S4 Binding assay results of E2 to GPR30 and validation of Lys05 induced GPR30 activation and Gq signaling.

(A) Binding assay results of [^{3}H]-E2 to GPR30 in Hi5 cell membrane, ERα as positive control. Data are mean ± S.E.M. from 3 independent experiments performed in duplicate (n = 3).

(B-C) Calcium assay and IP1 assay to validate Lys05, but not estrogen related compounds, induces GPR30 activation and Gq signaling. Data are mean ± S.E.M. from 3 independent experiments (n = 3).

Fig. S5

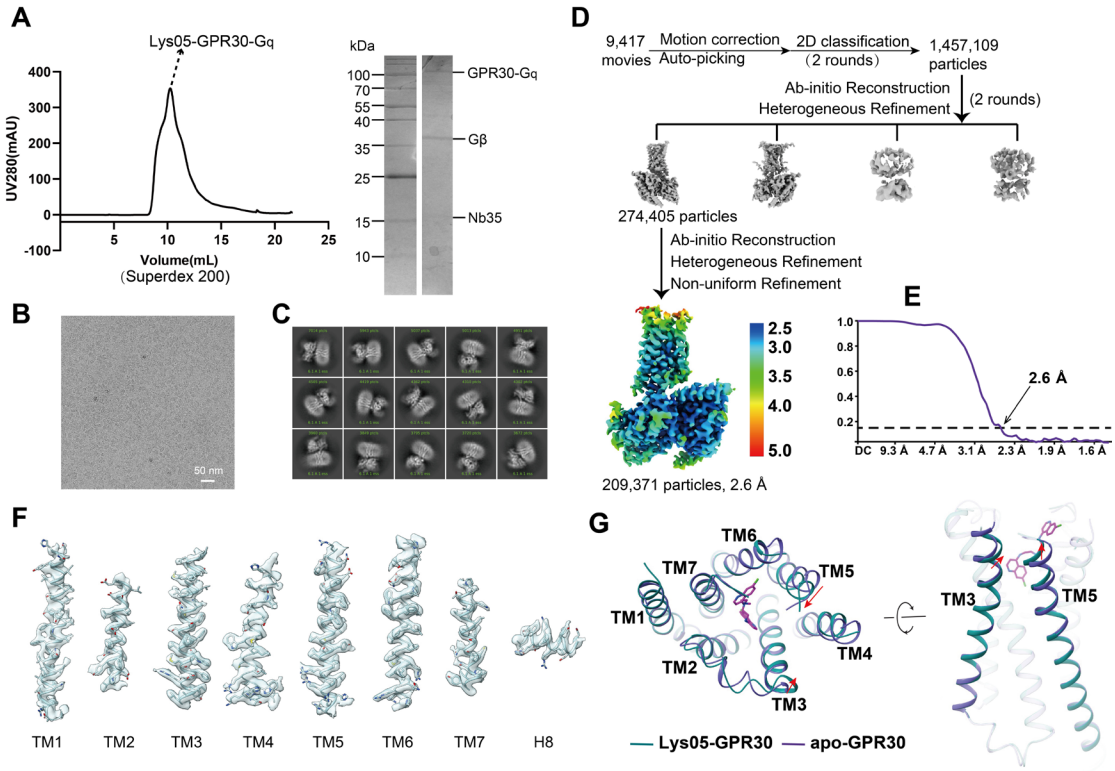

Fig. S5 Purification and structure determination of Lys05-GPR30-Gq complexes.

(A) Representative size exclusion chromatography (SEC) profiles and SDS-PAGE analysis of Lys-05 activated GPR30-Gq complex.

(B-C) Representative cryo-EM image (B) and 2D classification averages (C) of Lys05-GPR30-Gq complexes.

(D-E) Cryo-EM data processing flowcharts (D) and the Fourier shell correlation (FSC) curves (E) of Lys05-GPR30-Gq complexes. The global resolution of the final processed density map estimated at the FSC = 0.143 is 2.6 Å.

(F) The density maps of TM1–TM7 and helix 8(H8) of GPR30 in Lys05-GPR30-Gq complexes.

(G) Comparison of Lys05 bound and apo-GPR30 structures.

Fig. S6

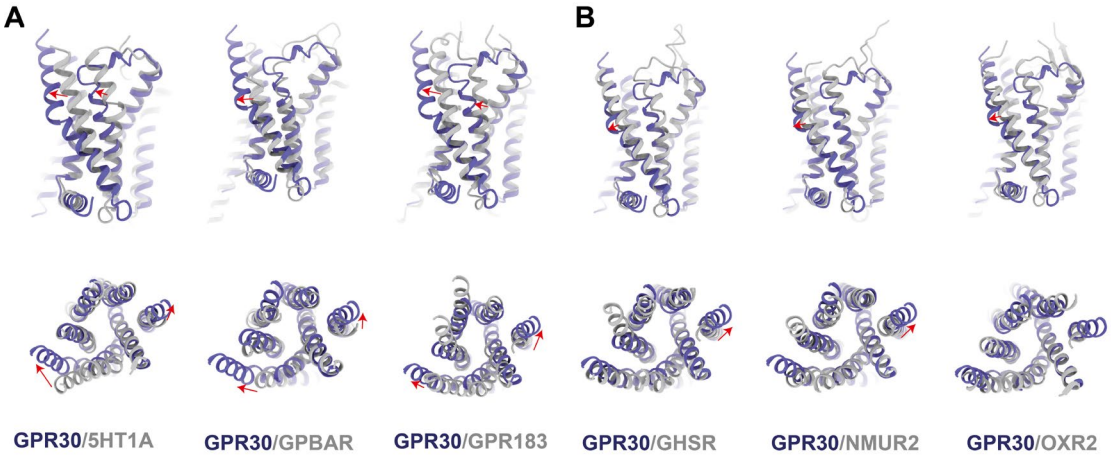

Fig. S6 Structural analysis reveals a unique distribution of the transmembrane region of GPR30.

(A) Structure comparison of GPR30's 7TM bundle with that of $5HT_{1A}$ (PDB code: 7E2Y), GPBAR (PDB code: 7CFM) and GPR183(PDB code: 7TUZ).

(A) Structure comparison of GPR30's 7TM bundle with that of GHSR (PDB code: 7F9Z), NMUR2 (PDB code: 7W55) and OXR2 (PDB code: 7L1U).

Fig. S7

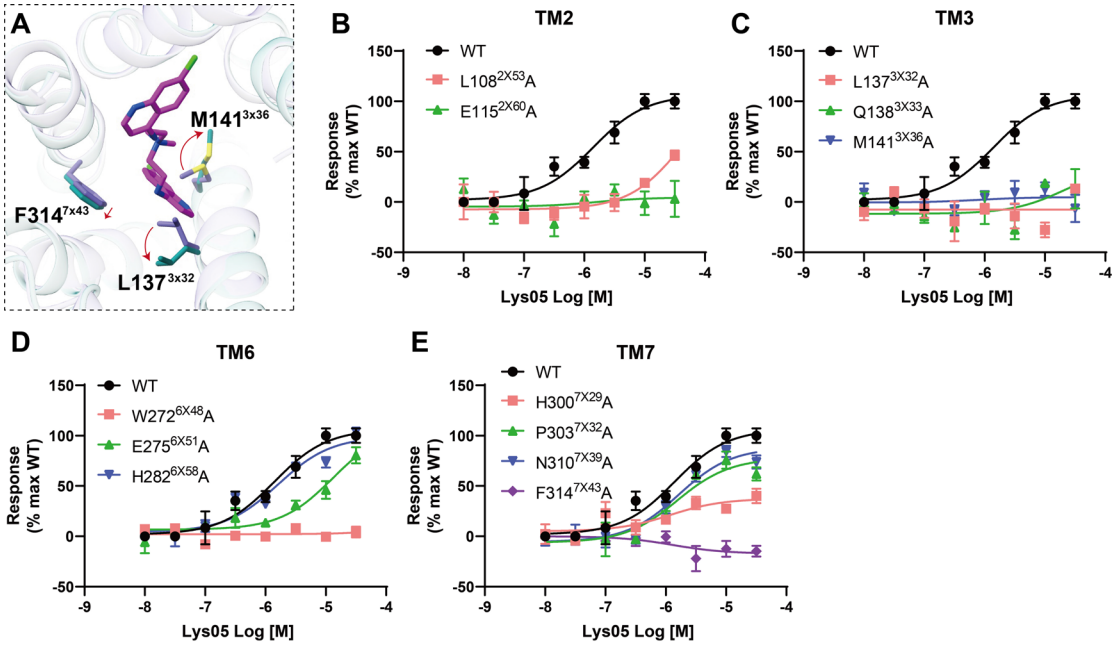

Fig. S7 Mutational effects of Lys05-GPR30 interacting residues to the activation of GPR30.

(A) Structure comparison of apo-GPR30 and Lys05-GPR30 indicated the conformational changes of related residues during Lys05 insertion.

(B-E) Dose-response curves of Lys05 in activating the mutated GPR30, mutations are located in TM2 (B), TM3 (C), TM6 (D), and TM7 (E). Data are mean ± S.E.M. from 3 independent experiments (n = 3).

Table S1 Cryo-EM data collection, refinement and validation statistics

	GPR30-Gq complex				
	E2	**G1**	**Ful**	**apo**	**Lys05**
Voltage (kV)	300	300	300	300	300
Electron exposure (e^-/Å^2)	50	50	50	50	50
Defocus range (μm)	-1.0 to -2.0	-1.0 to -2.0	-1.0 to -2.0	-1.0 to -2.0	-1.0 to -2.0
Pixel size (Å)	1.071	1.071	1.071	0.824	0.732
Symmetry imposed	C1	C1	C1	C1	C1
Filtered particle images (no.)	1,199,129	1,065,934	3,410,733	1,072,804	1,457,109
Final particle images (no.)	177,591	411,141	536,691	300,561	209,371
Map resolution (Å)	3.2	3.1	3.2	2.9	2.6
FSC threshold	0.143	0.143	0.143	0.143	0.143
Map resolution range (Å)	2.5 - 5.0	2.5 - 5.0	2.5 - 5.0	2.5 - 5.0	2.5 - 5.0
Refinement					
Initial model used (PDB code)	AlphaFold GPR30	AlphaFold GPR30	AlphaFold GPR30	AlphaFold GPR30	AlphaFold GPR30
Map sharpening *B* factor (Å^2)	-80	-147.6	-135.5	-104.4	-96.2
Model composition					
Non-hydrogen atoms	8,816	8,806	8,771	8,721	8,025
Protein residues	1,117	1,118	1,116	1,116	1,016
Ligands	0	0	0	0	1
B factors (Å^2)					
Protein	65.24	73.12	57.57	125.84	77.77
Ligand	- -	- -	- -	- -	114.37
R.m.s. deviations					
Bond lengths (Å)	0.003	0.003	0.003	0.004	0.003
Bond angles (°)	0.557	0.564	0.539	0.950	0.539
Validation					
MolProbity score	1.30	1.30	1.34	1.25	1.38
Clashscore	4.05	3.71	4.53	3.59	4.08
Poor rotamers (%)	0.00	0.00	0.00	0.00	0.00
Ramachandran plot					
Favored (%)	97.44	97.26	97.44	97.53	96.89
Allowed (%)	2.56	2.74	2.56	2.47	3.11
Disallowed (%)	0.00	0.00	0.00	0.00	0.00

Table S2. Effects of Lys05 on activation of GPR30 and its mutants.

Receptor	pEC_{50} [a]	Emax (%)[a]	Surface Expression (WT%) [b]
WT	5.88±0.12	100±7.3	100±17
$L108^{2X53}A$	4.33±0.19	46.6±4.75	105±1.5
$E115^{2X60}A$	UD [c]	10.5±7.0	142±25
$L137^{3X32}A$	UD	13.3±1.0	143±13
$Q138^{3X33}A$	UD	18.7±1.7	166±15
$M141^{3X36}A$	UD	12.7±6.8	114±5.1
$W272^{6X48}A$	UD	8.03±1.5	89.4±4.8
$E275^{6X51}A$	4.9±0.07	80.6±8.0	104±2.2
$H282^{6X58}A$	5.95±0.44	104±2.2	109±1.8
$H300^{7X29}A$	5.68±0.21	40.0±7.1	81.7±11
$P303^{7X32}A$	5.82±0.06	75.7±8.5	90.2±1.6
$N310^{7X39}A$	5.75±0.14	84.4±5.5	98.2±12
$F314^{7X43}A$	UD	0.61±3.9	98.4±2.9

[a] Data shown are means ± S.E.M. from at least three independent experiments.

[b] Data were normalized to the expression level of WT GPR30 in HEK293 cells. Data shown are means ± S.E.M. from four independent experiments.

[c] UD-undetectable, indicates that the activation level is too low to determine EC_{50} values.